On Uncertainty in Deep State Space Models for Model-Based Reinforcement Learning

Philipp Becker   *philipp.becker@kit.edu*
Autonomous Learning Robots Lab, Karlsruhe Institute of Technology

Gerhard Neumann   *gerhard.neumann@kit.edu*
Autonomous Learning Robots Lab, Karlsruhe Institute of Technology

Abstract

Improved state space models, such as *Recurrent State Space Models (RSSMs)*, are a key factor behind recent advances in model-based reinforcement learning (RL). Yet, despite their empirical success, many of the underlying design choices are not well understood. We show that *RSSMs* use a suboptimal inference scheme and that models trained using this inference overestimate the aleatoric uncertainty of the ground truth system. We find this overestimation implicitly regularizes *RSSMs* and allows them to succeed in model-based RL. We postulate that this implicit regularization fulfills the same functionality as explicitly modeling epistemic uncertainty, which is crucial for many other model-based RL approaches. Yet, overestimating aleatoric uncertainty can also impair performance in cases where accurately estimating it matters, e.g., when we have to deal with occlusions, missing observations, or fusing sensor modalities at different frequencies. Moreover, the implicit regularization is a side-effect of the inference scheme and not the result of a rigorous, principled formulation, which renders analyzing or improving *RSSMs* difficult. Thus, we propose an alternative approach building on well-understood components for modeling aleatoric and epistemic uncertainty, dubbed *Variational Recurrent Kalman Network (VRKN)*. This approach uses Kalman updates for exact smoothing inference in a latent space and Monte Carlo Dropout to model epistemic uncertainty. Due to the Kalman updates, the *VRKN* can naturally handle missing observations or sensor fusion problems with varying numbers of observations per time step. Our experiments show that using the *VRKN* instead of the *RSSM* improves performance in tasks where appropriately capturing aleatoric uncertainty is crucial while matching it in the deterministic standard benchmarks[1].

1 Introduction

Accurate system models are crucial for model-based control and reinforcement learning (RL) in autonomous systems applications under partial observability. Practitioners commonly use state space models (SSMs) (Murphy, 2012) to formalize such systems. SSMs consist of a dynamics model, describing how one state relates to the next, and an observation model, which describes how system states generate observations. Yet, dynamics and observation models are unknown for most relevant problems, and exact inference in the resulting SSM is usually intractable. Researchers have proposed numerous approaches to learn the models from data and approximate the inference to solve those issues.

Recurrent State Space Models (RSSMs) (Hafner et al., 2019) are of particular interest here. Using *RSSMs* as the backbone for their *Deep Planning Network (PlaNet)*, Hafner et al. (2019) showed that variational latent dynamics learning can succeed in image-based RL for complex control tasks. Combined with simple

---
[1]Code available at: https://github.com/pbecker93/vrkn

planning, *RSSMs* can match the performance of model-free RL while requiring significantly fewer environment interactions. The authors later improved upon their original model, including a parametric policy trained on imagined trajectories (*Dreamer*) (Hafner et al., 2020). In general, approaches based on *RSSM*s have found considerable interest in the model-based RL community. Yet, while *RSSM*s draw inspiration from classical SSMs, they use a simplified inference scheme. During inference, they assume the belief is independent of future observations instead of using the correct smoothing assumptions (Murphy, 2012) to obtain the belief. We formalize this observation in Section 2 and discuss how these simplified assumptions result in a theoretically looser variational lower bound. Further, we analyze the effects of these assumptions on model learning and find they cause an overestimation of aleatoric uncertainty. Such aleatoric uncertainty stems from partial observability or inherent stochasticity of the system (Hüllermeier & Waegeman, 2021). It plays an important role in many realistic tasks, e.g., in the form of occlusions, missing observations, or observations arriving in different modalities and frequencies. Consider, for example, low-frequency camera images providing external information and high-frequency proprioceptive measurements of the robot's internal state. Given such sensory inputs, we require an appropriate estimation of aleatoric uncertainty to fuse all information optimally and form accurate belief states. Our experiments show that *RSSMs* performance sub-optimally in such cases, which we attribute to the wrong estimation of aleatoric uncertainty.

Furthermore, we argue that the *RSSM's* inference assumptions are a double-edged sword for model-based RL. On the one hand, the overestimated aleatoric uncertainty can be beneficial as it leads to dynamics models that generalize better and are more robust to *objective mismatch* (Luo et al., 2019; Lambert et al., 2020). Such *objective mismatch* arises because the model aims to maximize the data likelihood while the metric we care about is the agent's reward. Additionally, as the agent explores during training, it will encounter states and actions the model has not seen, causing a distribution shift between training and data collection. While many approaches rely on explicit epistemic uncertainty to tackle this issue (Chua et al., 2018; Janner et al., 2019), *RSSMs* succeed without capturing epistemic uncertainty. Such epistemic uncertainty (Hüllermeier & Waegeman, 2021) stems from the lack of training data and plays an important role in model-based RL, where the data is not given but collected during the training process. On the other hand, this heuristic approach to address *objective mismatch* complicates the design and analysis of the approach as the robustness is a side-product of the inference scheme and does not follow well-motivated principles. For example, purely stochastic versions of the *RSSM* gives unsatisfactory results, and it is unclear why this is the case. Arguably, an explanation could be the overestimated aleatoric uncertainty causing the purely stochastic model to be unstable. As a remedy, Hafner et al. (2019) introduce a *deterministic path*, i.e., they combine stochastic and deterministic features to form the belief state.

We show that removing this issue for *RSSMs* by implementing a naive approach to smoothing yields unsatisfactory results, even if the model uses explicit epistemic uncertainty to compensate for the missing overestimation of the aleatoric uncertainty. To make smoothing inference work, we redesign the model using well-understood and theoretically founded components to model aleatoric and epistemic uncertainty. We dub the resulting model *Variational Recurrent Kalman Network (VRKN)*. It uses a linear Gaussian State Space Model embedded in a latent space, which allows closed-form smoothing inference and proper estimation of aleatoric uncertainty. Furthermore, as the inference builds on Bayes rule, it provides a natural treatment of missing observations and sensor fusion settings. Additionally, the *VRKN* uses Monte Carlo Dropout (Gal & Ghahramani, 2016) for a Bayesian treatment of its transition model's parameters, explicitly modeling epistemic uncertainty.

We first show that the resulting architecture allows model-based agents to perform comparably to *RSSM*-based agents on standard benchmarks from the Deep Mind Control Suite (Tassa et al., 2018). Those environments are almost deterministic, i.e., the aleatoric uncertainty is low. Subsequently, we modify tasks from the Deep Mind Control Suite to create three different scenarios which exhibit high aleatoric uncertainty, i.e., (i) we introduce occlusions, (ii) missing observations, and (iii) sensor fusions problems of external camera images and internal proprioceptive feedback which are available at different frequencies. Using those, we show that the *VRKN* improves the agents' performance due to its accurate estimation of aleatoric uncertainty. Our approach builds on well-motivated components for aleatoric and epistemic uncertainty. Additionally, it does not require heuristic model components such as a *deterministic path*. As such, it may serve as a basis for future research into improving state space models for model-based RL.

To summarize our contributions:

1. We analyze the assumptions underlying the *RSSM* and show that they are not only suboptimal but also have subtle effects on model learning. They lead to an overestimation of the aleatoric uncertainty (Section 2.1 and Section 2.2).

2. We argue that, counterintuitively, this suboptimal inference is beneficial for the *RSSMs* performance as it addresses *objective mismatch* in a heuristic way (Section 2.3). We evaluate several modifications to the *RSSM* to provide empirical evidence to support this hypothesis (Section 4.1).

3. We introduce the *VRKN*, providing a more principled inductive bias for smoothing inference than the *RSSM* (Section 3). We again show that a smoothing inference without additional measures results in suboptimal performance, yet, when combined with epistemic uncertainty, the *VRKN*'s improved inductive bias allows it to close the performance gap on standard benchmarks (Section 4.1).

4. We show that *VRKN*-based agents improve performance in tasks where correct uncertainty estimation matters. Here we consider tasks with partial observability, missing information, or tasks that require sensor fusion. (Section 4.2)

2 Inference and Learning in State Space Models

State Space Models (SSMs) (Murphy, 2012) assume that a sequence of observations $\mathbf{o}_{\leq T} = \{\mathbf{o}_t\}_{t=0\cdots T}$ is generated by a sequence of latent state variables $\mathbf{z}_{\leq T} = \{\mathbf{z}_t\}_{t=0\cdots T}$, given a sequence of actions $\mathbf{a}_{\leq T} = \{\mathbf{a}_t\}_{t=0\cdots T}$. In SSMs, each observation $\mathbf{o}_t$ is assumed to only depend on the current latent state $\mathbf{z}_t$ via an observation model $p(\mathbf{o}_t|\mathbf{z_t})$. Further, they assume the latent states are Markovian, i.e., each latent state only depends on its direct predecessor and the corresponding action via a dynamics model $p(\mathbf{z}_{t+1}|\mathbf{z}_t, \mathbf{a}_t)$. Finally, the initial state is distributed according to a distribution $p(\mathbf{z}_0)$. Figure 1a shows the corresponding graphical model. Typically, when inferring latent states from observations, we consider three different beliefs for each $\mathbf{z}_t$. Those are the prior $p(\mathbf{z}_t|\mathbf{o}_{\leq t-1}, \mathbf{a}_{\leq t-1})$, i.e., the belief before observing $\mathbf{o}_t$, the posterior, $p(\mathbf{z}_t|\mathbf{o}_{\leq t}, \mathbf{a}_{\leq t-1})$, i.e., the belief after observing $\mathbf{o}_t$, as well as the smoothed belief $p(\mathbf{z}_t|\mathbf{o}_{\leq T}, \mathbf{a}_{\leq T})$ which is conditioned on all future observations and actions, until the last time step T. We refer to those estimates as state-beliefs to distinguish them from dynamics distributions, which are con-

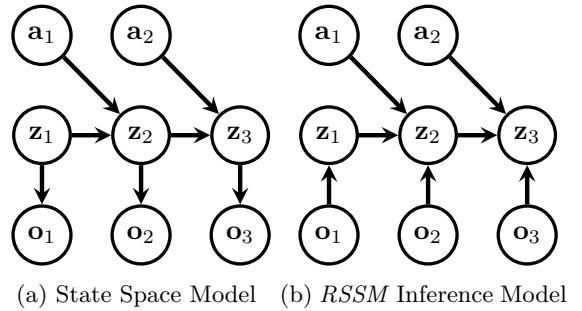(a) State Space Model   (b) *RSSM* Inference Model

Figure 1: (a) State space model, serving as the generative model throughout this work. (b) Graphical Model underlying the *RSSM* (Hafner et al., 2019) inference scheme. In contrast to the generative SSM, the direction between observations and latent states is inverted. These independence assumptions result in a simplified inference and subtle effects on model learning.

ditioned on the previous state $\mathbf{z}_{t-1}$ such as the prior dynamics $p(\mathbf{z}_t|\mathbf{z}_{t-1}, \mathbf{a}_{t-1})$, the posterior dynamics $p(\mathbf{z}_t|\mathbf{z}_{t-1}, \mathbf{o}_t, \mathbf{a}_{t-1})$ and the smoothed dynamics $p(\mathbf{z}_t|\mathbf{z}_{t-1}, \mathbf{o}_{\geq t}, \mathbf{a}_{\geq t-1})$. To get from a dynamics distribution to the corresponding state belief we need to marginalize out the previous state, e.g., $p(\mathbf{z}_t|\mathbf{o}_{\leq t-1}, \mathbf{a}_{\leq t-1}) = \int p(\mathbf{z}_t|\mathbf{z}_{t-1}, \mathbf{a}_{t-1})p(\mathbf{z}_{t-1}|\mathbf{o}_{\leq t-1}, \mathbf{a}_{\leq t-1})d\mathbf{z}_{t-1}$ for the prior.

Traditionally, the independence assumptions of the generative model, shown in Figure 1a, are also used for inference. Yet, *RSSMs* (Hafner et al., 2019) work with a different set of assumptions during inference, shown in Figure 1b[2]. In particular, in this graphical model the state $\mathbf{z}_t$ is conditionally independent of all observations $\mathbf{o}_{>t}$ and actions $\mathbf{a}_{\geq t}$ given $\mathbf{z}_{t-1}$, $\mathbf{a}_{t-1}$, and $\mathbf{o}_t$, which is not the case for the standard SSM. We

---

[2]The full model of Hafner et al. (2019) also includes a *deterministic-path* which is of no concern regarding the discussion here. Thus, we omit it for brevity. Furthermore, Hafner et al. (2019) compare their *RSSM* to a baseline they abbreviate as *SSM* (stochastic state model), which also builds on the simplified assumptions. In this work, we refer to all approaches based on the simplified assumptions as *RSSM*.

discuss the effects of those assumptions on inference and model learning. We refer to Appendix A for more detailed derivations of the following identities.

2.1 Variational Inference for State Space Models

Inferring beliefs over the latent states given observations and actions is intractable for most models. Thus, we usually use approximate inference methods. In this work, we focus on variational inference. Such variational methods introduce an auxiliary distribution q over the latent variables given the observable variables. They decompose the data log-likelihood into a variational lower bound and a Kullback-Leibler divergence (KL) term, measuring how close the bound is to the data log-likelihood. For State Space Models (SSMs) this decomposition is given as $\log p(\mathbf{o}_{\leq T}|\mathbf{a}_{\leq T}) =$

$$\underbrace{\mathbb{E}_{q(\mathbf{z}_{\leq T}|\mathbf{o}_{\leq T}, \mathbf{a}_{\leq T}))}\left[\log \frac{p(\mathbf{o}_{\leq T}, \mathbf{z}_{\leq T}|\mathbf{a}_{\leq T})}{q(\mathbf{z}_{\leq T}|\mathbf{o}_{\leq T}, \mathbf{a}_{\leq T})}\right]}_{\text{Lower Bound}} + \underbrace{\mathrm{KL}\left[q(\mathbf{z}_{\leq T}|\mathbf{o}_{\leq T}, \mathbf{a}_{\leq T}) \parallel p(\mathbf{z}_{\leq T}|\mathbf{o}_{\leq T}, \mathbf{a}_{\leq T})\right]}_{\text{KL term}(\geq 0)}. \tag{1}$$

Variational inference methods try to find the optimal q by maximizing the lower bound or minimizing the KL term. If a q can be found such that $q(\mathbf{z}_{\leq T}|\mathbf{o}_{\leq T}, \mathbf{a}_{\leq T}) = p(\mathbf{z}_{\leq T}|\mathbf{o}_{\leq T}, \mathbf{a}_{\leq T})$, the KL term is 0, and the bound is said to be tight. While the decomposition is valid for arbitrary distributions $q(\mathbf{z}_{\leq T}|\mathbf{o}_{\leq T}, \mathbf{a}_{\leq T})$, we need to pose a set of independence assumptions to obtain tractable variational models. If we again use the independence assumptions of the generative model, shown in Figure 1a, we can obtain the inference model by explicitly inverting the generative direction using Bayes rule, $q(\mathbf{z}_{\leq T}|\mathbf{o}_{\leq T}, \mathbf{a}_{\leq T}) = \frac{1}{p(\mathbf{o}_{\leq T})} p(\mathbf{z}_0) \prod_{t=1}^{T} p(\mathbf{z}_t|\mathbf{z}_{t-1}, \mathbf{a}_t) \prod_{t=0}^{T} p(\mathbf{o}_t|\mathbf{z}_t)$. For certain model parametrizations, this variational distribution can be computed analytically, e.g., by Kalman smoothing if the model is linear and Gaussian. In this case, the KL term vanishes, and the bound is tight.

Yet, *RSSMs*, as introduced in (Hafner et al., 2019), assume the variational distribution factorizes as

$$q(\mathbf{z}_{\leq T}|\mathbf{o}_{\leq T}, \mathbf{a}_{\leq T}) = q(\mathbf{z}_0|\mathbf{o}_0) \prod_{t=1}^{T} q(\mathbf{z}_t|\mathbf{z}_{t-1}, \mathbf{o}_t, \mathbf{a}_{t-1}).$$

This assumption results in a simplified inference procedure, as the belief over $\mathbf{z}_t$ is assumed to be independent of all future observations $\mathbf{o}_{>t}$, given $\mathbf{z}_{t-1}$, $\mathbf{o}_t$, and $\mathbf{a}_{t-1}$.

Inserting this assumptions into the KL term yields $\mathrm{KL}\left[q(\mathbf{z}_{\leq T}|\mathbf{o}_{\leq T}, \mathbf{a}_{\leq T}) \parallel p(\mathbf{z}_{\leq T}|\mathbf{o}_{\leq T}, \mathbf{a}_{\leq T})\right] =$

$$\sum_{t=1}^{T} \mathbb{E}_{q(\mathbf{z}_{t-1}|\mathbf{o}_{\leq t-1}, \mathbf{a}_{\leq t-2})}\left[\mathrm{KL}\left[q(\mathbf{z}_t|\mathbf{z}_{t-1}, \mathbf{o}_t, \mathbf{a}_{t-1}) \parallel p(\mathbf{z}_t|\mathbf{z}_{t-1}, \mathbf{o}_{\geq t}, \mathbf{a}_{\geq t-1})\right]\right]. \tag{2}$$

For general distributions p, the individual terms in this sum will not be 0, as the right-hand side distributions receive information, i.e., future observations and actions, which are ignored by the variational distribution. Thus, this bound can in general not be tight, not even for linear Gaussian models as the resulting variational distribution can in general not represent $p(\mathbf{z}_{\leq t}|\mathbf{o}_{\leq T}, \mathbf{a}_{\leq T})$. Typically, tight variational bounds are preferable as they allow for faster optimization of the marginal log-likelihood.

The above discussion may be hypothetical, as all considered architectures do not provide tight lower bounds due to the use of deep neural networks, which prevents analytic solutions for inference. Still, as a tight lower bound does not even theoretically exist for the *RSSM* assumptions, we believe this is already an indication of the misspecification of its inference distribution.

2.2 Model Learning under Different Inference Assumptions

In the model-based RL setting considered in this work, the generative model is usually assumed to be unknown and we jointly learn a parametric generative model $p_{\boldsymbol{\theta}}$ and an inference model q_{ψ} using an auto-encoding variational Bayes approach (Kingma & Welling, 2013; Sohn et al., 2015) by maximizing the lower

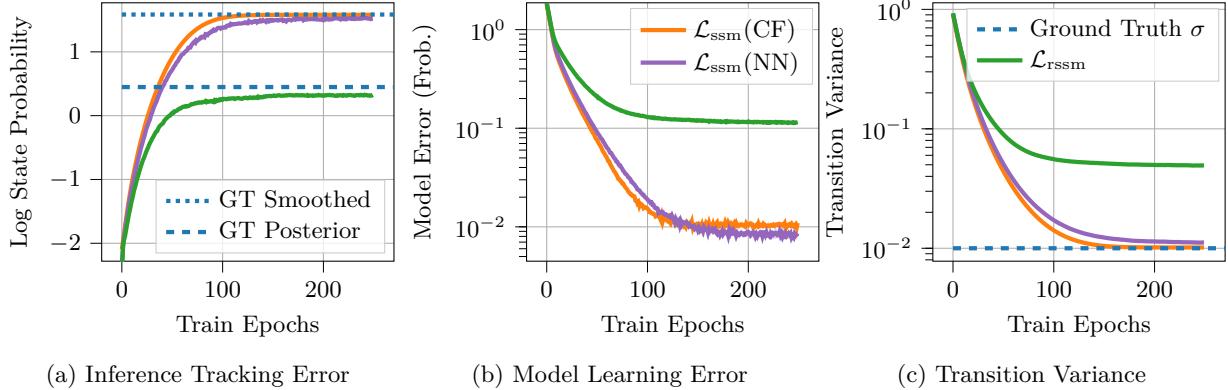(a) Inference Tracking Error   (b) Model Learning Error   (c) Transition Variance

Figure 2: Comparison of inference and model learning results on a simple linear-Gaussian state space model without actions, under both *RSSM* and SSM inference assumptions. We report average results over 10 seeds and error bars indicating 95% bootstrapped confidence intervals. Note that the error bars are too small to be visible. We consider both a closed-form (CF) version based on Kalman Smoothing and a version with a neural network (NN) as an inference model for the SSM-based approaches and find that only the objective matters, not the parametrization of the inference model. **(a)** Log-probability of the ground truth states under the learned models. We compare against the quality of the ground truth smoothed (GT Smoothed) and posterior (GT Posterior) beliefs, computed using a Kalman Smoother and ground truth generative model. While the SSM objective reaches the quality of the smoothed belief, the *RSSM*-based inference fails to attain the quality of even the posterior belief. **(b)**: Distance between ground truth transition matrix and learned transition matrix, measured using the Frobenius norm. Here, the SSM inference yields a model that is an order magnitude closer to the ground-truth model than that learned by the *RSSM*-bound. **(c)**: Transition variance $\tilde{\sigma}\mathbf{I}$. With the SSM bound we recover the ground-truth aleatoric uncertainty, yet with the *RSSM* bound the aleatoric uncertainty is significantly overestimated.

bound part of Equation 1. Inserting the *RSSM*-assumptions into the general lower bound gives the objective introduced by Hafner et al. (2019), $\mathcal{L}_{\mathrm{rssm}}(\mathbf{o}_{\leq T}, \mathbf{a}_{\leq T}) =$

$$\sum_{t=1}^{T} \mathbb{E}_{q_{\boldsymbol{\psi}}(\mathbf{z}_t|\mathbf{o}_{\leq t}, \mathbf{a}_{\leq t})} \left[\log p_{\boldsymbol{\theta}}(\mathbf{o}_t|\mathbf{z}_t)\right] - \mathbb{E}_{q_{\boldsymbol{\psi}}(\mathbf{z}_{t-1}|\mathbf{o}_{\leq t-1}, \mathbf{a}_{\leq t-1})} \left[\mathrm{KL}\left[q_{\boldsymbol{\psi}}(\mathbf{z}_t|\mathbf{z}_{t-1}, \mathbf{a}_{t-1}, \mathbf{o}_t) \,\|\, p_{\boldsymbol{\theta}}(\mathbf{z}_t|\mathbf{z}_{t-1}, \mathbf{a}_{t-1})\right]\right]. \quad (3)$$

If one instead uses the same factorization assumptions as the generative model, the inference distribution factorizes as $q_{\boldsymbol{\psi}}(\mathbf{z}_{\leq T}|\mathbf{o}_{\leq T}, \mathbf{a}_{\leq T}) = q_{\boldsymbol{\psi}}(\mathbf{z}_0|\mathbf{o}_{\leq T}, \mathbf{a}_{\leq T}) \prod_{t=1}^{T} q_{\boldsymbol{\psi}}(\mathbf{z}_t|\mathbf{z}_{t-1}, \mathbf{a}_{\geq t-1}, \mathbf{o}_{\geq t})$. Inserting this factorization into the general lower bound leads to $\mathcal{L}_{\mathrm{ssm}}(\mathbf{o}_{\leq T}, \mathbf{a}_{\leq T}) =$

$$\sum_{t=1}^{T} \mathbb{E}_{q_{\boldsymbol{\psi}}(\mathbf{z}_t|\mathbf{o}_{\leq T}, \mathbf{a}_{\leq T})} \left[\log p_{\boldsymbol{\theta}}(\mathbf{o}_t|\mathbf{z}_t)\right] - \mathbb{E}_{q_{\boldsymbol{\psi}}(\mathbf{z}_{t-1}|\mathbf{o}_{\leq T}, \mathbf{a}_{\leq T})} \left[\mathrm{KL}\left[q_{\boldsymbol{\psi}}(\mathbf{z}_t|\mathbf{z}_{t-1}, \mathbf{a}_{\geq t-1}, \mathbf{o}_{\geq t}) \,\|\, p_{\boldsymbol{\theta}}(\mathbf{z}_t|\mathbf{z}_{t-1}, \mathbf{a}_{t-1})\right]\right]. \quad (4)$$

Opposed to the *RSSM*-objective, this objective uses the smoothed belief-state $q_{\boldsymbol{\psi}}(\mathbf{z}_t|\mathbf{o}_{\leq T}, \mathbf{a}_{\leq T})$ and the smoothed dynamics $q_{\boldsymbol{\psi}}(\mathbf{z}_t|\mathbf{z}_{t-1}, \mathbf{a}_{\geq t-1}, \mathbf{o}_{\geq t})$. The variational distribution considers all future information until $t = T$ and thus can theoretically yield a tight bound.

These differences have interesting effects on the learned transition model $p_{\boldsymbol{\theta}}(\mathbf{z}_t|\mathbf{z}_{t-1}, \mathbf{a}_{t-1})$. For the *RSSM*, the belief over past states can, by definition, not change due to additional observations. Thus, any discrepancy between this past belief and the current observation must be explained by the transition model. In contrast, a smoothing inference can also explain the discrepancy by propagating information from observations to past beliefs. In Equation 3, this observation is reflected in the expected KL-term, where the expectation does not consider $\mathbf{o}_t$ or other future observations. Thus, the transition model has to explain the transitions from a given $\mathbf{z}_{t-1}$ to $\mathbf{z}_t$, even if $\mathbf{z}_{t-1}$ would be rendered implausible by a future observation.

For a thought experiment illustrating these effects, consider the following scenario. You meet a person holding a box, and they tell you there is a hamster inside. As your prior experience is that people are

usually trustworthy, you chose to believe them. Next, the box opens, and a cat jumps out. As you trust your eyes, you now believe it is a cat. Yet, under the *RSSM*-assumptions, you cannot revise your belief of the first time step and thus still believe it originally was a hamster. When updating your model based on this interaction, you would learn that hamsters can turn into cats, as you cannot capture the arguably more likely explanation that the person lied. Learning under these assumptions requires you to model unlikely events as more likely than they are. Thus, you overestimate the aleatoric uncertainty in the world.

More formally, we can demonstrate this effect using a simple linear-Gaussian State Space Model without actions. We will use a state dimension of 4 and the ground-truth generative model given by

$$p(\mathbf{z}_0) = \mathcal{N}(\mathbf{z}_0|\mathbf{0}, \mathbf{I}), \quad p(\mathbf{o}_t|\mathbf{z}_t) = \mathcal{N}(\mathbf{o}_t|\mathbf{Iz}_t, 0.025\mathbf{I}), \quad p(\mathbf{z}_{t+1}|\mathbf{z}_t) = \mathcal{N}(\mathbf{z}_{t+1}|\mathbf{Az}_t, 0.01\mathbf{I})$$

where $\mathbf{I}$ denotes the identity matrix. The transition matrix $\mathbf{A}$ induces a slightly damped, oscillating behavior. The complete matrix $\mathbf{A}$, together with further details regarding the exact setup of this experiment, can be found in Appendix B. Using this generative model, we generate $1,000$ sequences of length 50. Even in this simple setting, computing the optimal inference distribution for the *RSSM*-bound (Equation 3) is impossible, and we thus resort to numerical methods. We parameterize $q_{\boldsymbol{\psi}}(\mathbf{z}_t|\mathbf{z}_{t-1}, \mathbf{o}_t)$ as locally linear-Gaussian distributions and learn the parameters using a neural network. For the SSM-bound (Equation 4 we can either compute the optimal inference in closed form, or again parameterize $q_{\boldsymbol{\psi}}(\mathbf{z}_t|\mathbf{z}_{t-1}, \mathbf{o}_{\geq t})$ as a neural network. To condition on future observations, we use a GRU (Cho et al., 2014) which runs backward over the observation sequence. For the generative model, we learn a transition matrix $\tilde{\mathbf{A}}$ and an isotropic covariance $\tilde{\sigma}\mathbf{I}$ jointly with the parameters of the inference model, i.e., $\boldsymbol{\theta} = \{\tilde{\mathbf{A}}, \tilde{\sigma}\}$. We fix the remaining parts of the generative model to the ground-truth values. Figure 2 summarizes the results and demonstrates that the *RSSM*-bound leads to a suboptimal inference and consequently to learning a wrong model. In particular, we can see that for the *RSSM*, the transition variance $\tilde{\sigma}$ is much larger than the ground-truth value $\sigma = 0.01$ as all unexpected observations have to be explained by the transitions instead of correcting the beliefs of past time steps.

2.3 The Interplay of Policy Optimization and Regularization

Despite the theoretical considerations in the previous section, *RSSMs* work well for model-based RL. It is well known that model-based RL suffers from an *objective mismatch* (Luo et al., 2019; Lambert et al., 2020) issue. This issue arises because the model aims to maximize the ELBO (Equation 1) but is evaluated based on the agent's reward. The effect is further amplified by the distribution shift between training and data collection, as data collection is typically performed only after a policy improvement step. In RL, we explicitly want the agent to explore unseen parts of the state-action space, encountering observations the model has not seen before. Thus, training the underlying model requires careful regularization such that wrong predictions do not prevent the agent from exploring relevant parts of the state space. Many model-based RL approaches (Chua et al., 2018; Janner et al., 2019) handle this issue by explicitly modeling the epistemic uncertainty of the model, which is not required by the *RSSM*. Instead, we argue that *RSSMs* rely on the overestimated aleatoric uncertainty caused by suboptimal inference to address *objective mismatch* in a more heuristic manner. The overestimation implicitly regularizes the *RSSM* as it forces the transition model to model unlikely events with higher probability. This regularization thus implicitly prevents overconfident model predictions due to overfitting. Yet, while it alleviates the *objective mismatch* issue, there are also drawbacks to this heuristic solution. First, it complicates the model design, analysis, and improvement of *RSSMs*. As already observed by Hafner et al. (2019), a fully stochastic model based on the *RSSM*-assumptions underperforms without additional measures as it fails at reliably propagating information for multiple time steps. As a remedy, Hafner et al. (2019) introduce a *deterministic-path*, i.e., a Gated Recurrent Unit (Cho et al., 2014), and base the belief update on this instead of the stochastic belief. Second, as we show in Section 4.2, there are settings where appropriately capturing the aleatoric uncertainty is important, and failing to do so can hurt performance.

In a first attempt to address those issues, we minimally adapt the *RSSM* to be capable of smoothing. This Smoothing *RSSM* uses a GRU which is added before the actual *RSSM* and runs backwards over the representations extracted by the encoder, effectively accumulating all future information. The *RSSM* then receives the output of this GRU instead of the original observation as input. This model is an extension of the
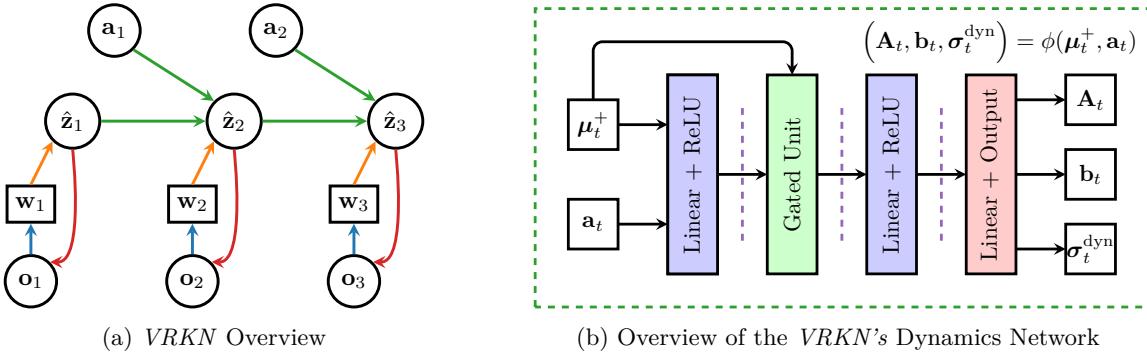
(a) *VRKN* Overview

(b) Overview of the *VRKN's* Dynamics Network

Figure 3: **(a)** We use an encoder (blue) to extracts an intermediate representation $\mathbf{w}_t$ and the observation noise $\boldsymbol{\sigma}_t^{\mathbf{w}}$ from the original observation $\mathbf{o}_t$. Both, $\mathbf{w}_t$ and $\boldsymbol{\sigma}_t^{\mathbf{w}}$, are then used to update the state estimate $\hat{\mathbf{z}}_t$ using the closed-form Kalman belief update (Bayes rule for Gaussians) (orange). A decoder (red) reconstructs the observation given a state sample. We propagate the latent state estimate to the next time step using the transition model $p_{\boldsymbol{\theta}}(\mathbf{z}_{t-1}|\mathbf{z}_t, \mathbf{a}_{t-1})$ (green). The parameters of this distribution, $\mathbf{A}_t$, $\mathbf{b}_t$, and $\boldsymbol{\sigma}_t^{\mathrm{dyn}}$, are computed using the network $\phi(\boldsymbol{\mu}_t^+, \mathbf{a}_t)$, shown in **(b)**. The network receives the current posterior mean $\boldsymbol{\mu}_t^+$ and the action $\mathbf{a}_t$ as inputs. Thus, the resulting dynamics are linearized around the posterior mean, which allows closed-form belief propagation, similar to an extended Kalman Filter. For stability during training, the network includes a gated unit, i.e., a GRU cell, which receives the posterior mean $\boldsymbol{\mu}_t^+$ at the memory input. For a Bayesian treatment of the transition model's parameters, we include Monte Carlo Dropout layers at the positions indicated by the purple dashed lines.

neural network based inference model for $\mathcal{L}_{\mathrm{ssm}}$, introduced in the previous section ($\mathcal{L}_{\mathrm{ssm}}(\mathrm{CF})$ in Figure 1). We compare this approach to the original *RSSM* and present the results in Section 4.1, in particular Figure 4. Those results show that the performance decreases compared to the original *RSSM*. We argue that with a proper inference, the overestimated aleatoric uncertainty no longer regularizes the model, making it more prone to *objective mismatch*. Following other methods, we try to improve the results by modeling epistemic uncertainty. To this end, we use Monte Carlo Dropout (MCD) but find that it does not help to improve the Smoothing *RSSM's* performance. From these results, again presented in Figure 4, we conclude that solely addressing the suboptimal inference assumption is insufficient, but we also need to rethink the model's parameterization. We postulate that the additional GRU for the backward pass is a poor inductive bias and that we require a smoothing approach that adds as little complexity as possible to the model. In the next section, we will introduce an architecture that allows for parameter-free smoothing.

3 Variational Recurrent Kalman Networks

To provide a theoretically better-grounded alternative to the *RSSM*, we require a model which allows tractable inference while still scaling to complex image-based control tasks. Further, the architecture should allow efficient computation of smoothed and posterior state beliefs and dynamics. While we need smoothed beliefs for training, we require (filtered) posteriors for online control. In particular, as only the smoothed beliefs are explicitly used for training, the model needs to provide a strong inductive bias that enables it to still produce reasonable posterior estimates.

To meet these criteria, we introduce a new parametrization of the latent dynamics based on a linear-Gaussian state space model (LGSSM) (Murphy, 2012) embedded in a latent space. The linear-Gaussian assumptions allow a rigorous treatment of uncertainties while working in a learned latent space allows for modeling high-dimensional and non-linear systems. Inference in this LGSSM amounts to (extended) Kalman filtering and smoothing, enabling smoothing inference without introducing additional parameters besides the latent observation and dynamics model. Due to this property, the architecture can perform proper smoothing inference for training and also produce reasonable posterior beliefs for online control. As an additional benefit, the formulation can naturally handle missing observations and the fusion of multiple sensors, making it amenable to many realistic problems. To include epistemic uncertainty in our approach, we use Monte

Carlo Dropout (Gal & Ghahramani, 2016) for a Bayesian treatment of the LGSSM's transition model. We name the resulting approach *Variational Recurrent Kalman Network (VRKN)*. Figure 3 shows a schematic overview.

In the following, we first introduce the *VRKN*'s dynamics model, which is shared between the inference and generative parts of the model. Next, we introduce the parameterization of the inference model q_{ψ} and the generative model p_{θ}. We describe how to train the model and use it for control and conclude by elaborating on the natural fusion mechanism.

3.1 The *VRKN*'s Dynamics Model

Both, the *VRKN*'s inference model q_{ψ} and the generative model p_{θ}, use the same dynamics model. Such parameter sharing is common for variational time-series models (Karl et al., 2016; Fraccaro et al., 2017; Hafner et al., 2019; Klushyn et al., 2021), as it simplifies the architecture, reduces the number of parameters, and simplifies training.

We model the latent dynamics as

$$p_{\theta}(\mathbf{z}_{t+1}|\mathbf{z}_t, \mathbf{a}_t) = \mathcal{N}\left(\mathbf{z}_{t+1}|\mathbf{A}_t(\boldsymbol{\mu}_t^+, \mathbf{a}_t)\mathbf{z}_t + \mathbf{b}_t(\boldsymbol{\mu}_t^+, \mathbf{a}_t), \boldsymbol{\sigma}_t^{\mathrm{dyn}}(\boldsymbol{\mu}_t^+, \mathbf{a}_t)\right),$$

where $\boldsymbol{\mu}_t^+$ denotes the mean of the posterior state estimate $q_{\psi}(\mathbf{z_t}|\mathbf{o}_{\leq t}, \mathbf{a}_{\leq t})$ provided by the inference model. Thus, we learn a linearized dynamics around the current posterior mean. This parametrization builds on the work of Shaj et al. (2020), who propose using a model that is locally linear in the state while depending non-linearly on the action. Building on the assumption that there is no uncertainty in the actions, it is maximally flexible while still allowing the usage of extended Kalman filtering (Jazwinski, 1970). Here, the linearization around the current posterior mean $\boldsymbol{\mu}_t^+$ enables closed-form propagation of state beliefs.

We model $\mathbf{A}_t$ to be a diagonal matrix which is emitted together with the offset term $\mathbf{b}_t$ and the transition noise $\boldsymbol{\sigma}_t^{\mathrm{dyn}}$ by a single neural network $\left(\mathbf{A}_t, \mathbf{b}_t, \boldsymbol{\sigma}_t^{\mathrm{dyn}}\right) = \phi(\boldsymbol{\mu}_t^+, \mathbf{a}_t)$. We carefully design this network to prevent the state estimates and gradients from growing indefinitely during training. First, as $\mathbf{A}_t$ is diagonal, its values are its eigenvalues, and constraining them in an appropriate range ensures stable dynamics. To this end, we use an activation of the form $f(x) = s \cdot \mathrm{sigmoid}(x+b) + m$ where we choose s, b, and m such that it saturates at 0.1 and 0.99 while $f(0) = 0.9$. Here, the intuition is that we want plausible and stable dynamics, which we initialize as a slightly dampened system. Second, we employ a gating mechanism to mitigate problems with vanishing and exploding gradients. To this end, we use a standard GRU cell implementation but feed the posterior mean $\boldsymbol{\mu}_t^+$ into the memory input, i.e., $\phi(\boldsymbol{\mu}_t^+, \mathbf{a}_t) = \phi_2(\mathrm{GRU}(\phi_1(\boldsymbol{\mu}_t^+, \mathbf{a}_t), \boldsymbol{\mu}_t^+))$. The resulting model is still fully stochastic and linear in $\mathbf{z}_t$. In contrast to the *RSSM*, it does not use a *determinstic-path* as the GRU cell does not introduce an additional deterministic memory and is used solely for addressing problems arising from unstable dynamics and gradients. We empirically found this helpful and took inspiration from standard recurrent architectures (Hochreiter & Schmidhuber, 1997; Cho et al., 2014), where gating mechanisms are a well-known approach to mitigate instabilities. Figure 3b provides an overview of the dynamics model architecture.

Modeling Epistemic Uncertainty. As discussed in Section 2.3, the overestimated aleatoric uncertainty of the *RSSM*'s transition model avoids overconfident estimates due to overfitting and compensates for the lack of explicit epistemic uncertainty. Thus, as our approach captures the aleatoric uncertainty correctly, we need to explicitly consider epistemic uncertainty to obtain a model that is also useable for policy optimization. We use Monte Carlo Dropout (Gal & Ghahramani, 2016) due to its simplicity and include corresponding layers at appropriate points in the transition model. Those point are shown in Figure 3b.

3.2 Inference Model

We aim for a model that can work with high-dimensional observations which depend non-linearly on the latent state while still allowing efficient inference of filtered and smoothed beliefs. Thus, we introduce an auxiliary, intermediate representation $\mathbf{w}_t$ for the original observations $\mathbf{o}_t$. Such an intermediate representation allows

us to capture the highly complex relations between state and observations in the mapping from $\mathbf{o}_t$ to $\mathbf{w}_t$ while using a simple observation model $q_{\psi}(\mathbf{w}_t|\mathbf{z}_t)$ in the latent space. This approach is common for variational latent state space models (Karl et al., 2016; Fraccaro et al., 2017; Klushyn et al., 2021) as it enables efficient inference in latent space. These approaches model $\mathbf{w}_t$ as a latent Gaussian random variable and learn it's mean and variance based on $\mathbf{o}_t$. They then sample $\mathbf{w}_t$ given these parameters. Yet, this assumption complicates inference and training, as now an additional latent variable, $\mathbf{w}_t$, has to be addressed. Further, it makes uncertainty propagation from observations to states harder (Becker et al., 2019; Volpp et al., 2021), as explicit uncertainty information is lost during sampling. Thus, following (Haarnoja et al., 2016; Becker et al., 2019; Shaj et al., 2020; Volpp et al., 2021), we instead formulate the observation model as $q_{\psi}(\mathbf{w}_t|\mathbf{z}_t) = \mathcal{N}\left(\mathbf{w}_t|\mathbf{z}_t, \boldsymbol{\sigma}_t^{\mathbf{w}}\right)$, where $\mathbf{w}_t = \mathrm{enc}_o(\mathbf{o}_t)$ and the diagonal covariance $\boldsymbol{\sigma}^{\mathbf{w}_t} = \mathrm{enc}_{\sigma}(\mathbf{o}_t)$ are given by an encoder network taking the original observation. In practice, the encoder consists of a single neural network with two output heads. This formulation does not suffer from the previously mentioned issues. First, as it models $\mathbf{w}_t$ as a direct mapping of the observation and not a random variable, we do not need to infer $\mathbf{w}_t$ but can assume it is observable. This assumption results in a simplified inference and training objective as we do not have to account for unobserved latent variables other than the latent state itself. Second, the encoder can directly extract the uncertainty in the observation, which tells the inference procedure how much it can rely on $\mathbf{w}_t$. For example, when estimating $\mathbf{w}_t$ from images, some images might contain certain information, e.g., the positions of an object, while others do not. The former case would result in a low uncertainty and the latter in a high one. Given $\mathbf{w_t}$ and $\boldsymbol{\sigma}_t^{\mathbf{w}}$ we can update belief states using the Kalman update, i.e., Bayes rule for Gaussian distributions,

$$q_{\psi}(\mathbf{z}_t|\mathbf{o}_{\leq t}, \mathbf{a}_{\leq t-1}) = \frac{1}{Z} q_{\psi}(\mathrm{enc}_o(\mathbf{o}_t)|\mathbf{z}_t) q_{\psi}(\mathbf{z}_t|\mathbf{o}_{\leq t-1}, \mathbf{a}_{\leq t-1}).$$

Here, $\boldsymbol{\sigma}_t^{\mathrm{w}}$ contributes to the computation of the Kalman gain, which highlights how the model uses the encoder's uncertainty to trade-off information from the prior belief and observation

The inference observation model is combined with the shared locally linear dynamics model $q_{\psi}(\mathbf{z}_{t+1}|\mathbf{z}_t, \mathbf{a}_t) = p_{\boldsymbol{\theta}}(\mathbf{z}_{t+1}|\mathbf{z}_t, \mathbf{a}_t)$ to obtain a latent LGSSM for inference. Given this dynamics model, we can forward beliefs in time using closed-form Gaussian marginalization,

$$q_{\psi}(\mathbf{z}_{t+1}|\mathbf{o}_{\leq t}, \mathbf{a}_{\leq t}) = \int q_{\psi}(\mathbf{z}_{t+1}|\mathbf{z}_t, \mathbf{a}_t) q_{\psi}(\mathbf{z}_t|\mathbf{o}_{\leq t}, \mathbf{a}_{\leq t-1}) d\mathbf{z}_t.$$

Repeating the described forms of forwarding beliefs in time and updating them based on observations amounts to standard (extended) Kalman filtering (Kalman, 1960; Jazwinski, 1970). Similarly, given these models, we can compute smoothed belief states using the Rauch-Tung-Striebel (Rauch et al., 1965) equations. In particular, the smoothing only requires beliefs and transition models computed during filtering and does not introduce additional learnable parameters. Note that both the filtering and smoothing equations simplify under our assumptions of diagonal covariances and are thus efficient and scalable. Thus, the smoothing inference only slightly increases the computational load during training. Especially in the image-based settings considered here, the computational cost largely stems from encoding and reconstructing observations.

3.3 Generative Model

Recall that we assume a generative State Space Model consisting of three parts. Those are the dynamics model, the observation model, and the initial state distribution. First, we have the dynamics model $p_{\boldsymbol{\theta}}(\mathbf{z}_{t+1}|\mathbf{z}_t, \mathbf{a}_t)$ as described in Section 3.1. Second, we assume a Gaussian generative observation model $p_{\boldsymbol{\theta}}(\mathbf{o}_t|\mathbf{z}_t)$ parameterized by a neural network (decoder). Following Hafner et al. (2019), we parameterize the mean by a neural network and assume a fixed variance. This parameterization is often empirically beneficial, especially in the image-based setting considered in our experiments, but not a theoretical constraint. We could also parameterize the variance by the network if required. Third, we have an initial state distribution $p_{\boldsymbol{\theta}}(\mathbf{z}_0)$. Here we use a Gaussian with zero mean and a learned diagonal variance which we initialize with the identity matrix.

3.4 Stochastic Gradient Variational Bayes for Model Learning

We train our model using a version of stochastic gradient variational Bayes (Kingma & Welling, 2013) and maximize $\mathcal{L}_{\text{ssm}}$, (Equation 4). Like most approaches building on (Kingma & Welling, 2013) we approximate all expectations in Equation 4 using Monte Carlo estimation with a single sample from the latent variable and jointly optimize the parameters of $q_{\boldsymbol{\psi}}$ and $p_{\boldsymbol{\theta}}$. For training, we infer the required belief states using the Kalman-based smoothing procedure described in Section 3.2. To compute the KL term in Equation 4 we additionally need the smoothed dynamics $q_{\boldsymbol{\psi}}(\mathbf{z}_{t+1}|\mathbf{z}_t, \mathbf{a}_{\geq t}, \mathbf{o}_{\geq t+1})$ which we obtain with minimal overhead by extending the RTS equations as detailed in subsection A.2.

The *VRKN's* formulation tightly couples posterior and smoothed beliefs by a fixed (not learned), deterministic, and well-motivated procedure. Smoothing using the Rauch-Tung-Striebel equations ensures that reasonable smoothed beliefs can only stem from reasonable posterior beliefs. Thus, while the posterior belief is not explicitly part of the objective, it is still learned during training as a prerequisite of the smoothed beliefs.

3.5 Using the Model for Online Control and Reinforcement Learning

When using the model for online control, we cannot smooth but have to act based on samples from the posterior belief $q_{\boldsymbol{\psi}}(\mathbf{z}_t|\mathbf{a}_{\leq t}, \mathbf{o}_{\leq t})$. We can rely on Kalman filtering, as described in Section 3.2, to obtain this posterior belief and omit the smoothing step, as future observations are unavailable. For the *VRKN*, the tight coupling between smoothed and posterior beliefs ensures the posteriors are reasonable and usable for control.

To act based on the latent state beliefs, we add a decoder network to predict rewards from latent states. Following (Hafner et al., 2019), this decoder is trained by adding a reconstruction loss term to the objective. Given the predicted reward, various forms of control are applicable to act optimally. Yet, in this work, we focus on the underlying state space model and thus reuse two previously introduced methods building on the *RSSM* (Hafner et al., 2019; 2020). The *PlaNet* (Hafner et al., 2019) approach plans actions using the cross entropy method by rolling out trajectories on the model. The *Dreamer* (Hafner et al., 2020) approach learns a parametric policy and value function based on latent imagination. Such latent imagination uses the model as a differentiable simulator and optimizes the policy based on the estimated values of predicted future states.

3.6 Sensor Fusion

Given the possibility of using the Kalman update for incorporating observations, we can use the *VRKN* for a simple but principled approach to sensor fusion. Formally, we assume the observation $\mathbf{o}_t$ factorizes into K different observations $\mathbf{o}_t^{(k)}$, i.e., $p_{\boldsymbol{\theta}}(\mathbf{o}_t|\mathbf{z}_t) = \prod_{k=1}^{K} p_{\boldsymbol{\theta}}(\mathbf{o}_t^{(k)}|\mathbf{z}_t)$. Those observations can be of various modalities and be available at different frequencies, e.g., high-frequency velocity information from an inertial measurement unit and low-frequency camera images of the surroundings. In this scenario, we have K encoders and K decoders, one for each $\mathbf{o}_t^{(k)}$. Similar to more traditional sensor fusion approaches (Gustafsson, 2010), we then accumulate the intermediate observation representation $\mathbf{w}_t^{(k)}$ by repeatedly applying the Kalman update. This approach reflects the invariance to permutations of all observations for a single time step. Furthermore, it enables the model to omit the update if some of the K observations are unavailable for a time step.

4 Evaluation

We compare the *VRKN*, the original *RSSM*, and the modified *RSSM* version introduced in Section 2.3 on image-based continuous control tasks using the DeepMind Control Suite (Tassa et al., 2020). Prior works (Lambert et al., 2020; Lutter et al., 2021) concluded that the model's predictive performance is often uninformative about the quality of the model-based agent. We concluded the same after preliminary experiments and want to study the effects of the different assumptions and parametrizations on the performance in a model-based RL setting. Thus, we evaluate the state space models as backbones for model-based
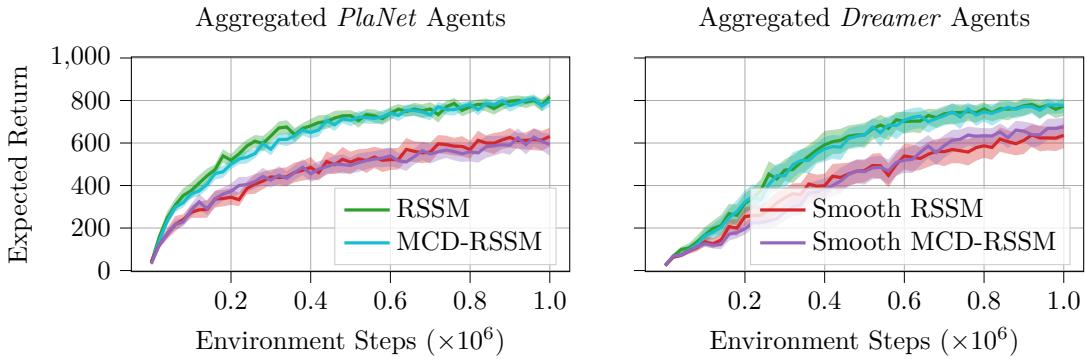
Figure 4: Comparison of the *RSSM*, the simple smoothing extension (Smooth *RSSM*) as well as versions of both models using Monte Carlo Dropout (MCD) to capture epistemic uncertainty in the dynamics (MCD-*RSSM* and Smooth MCD-*RSSM*). Note that we use different tasks for *PlaNet* and *Dreamer*-based agents. Thus the left and right plots are not directly comparable. For both types of agents, we find that proper inference by smoothing deteriorates performance. The additional epistemic uncertainty does not compensate for this decrease in performance.

agents and directly consider the achieved reward. As mentioned, we use both the *PlaNet* and the *Dreamer* approaches for control and thus closely follow the experiment setup described by Hafner et al. (2019; 2020). Appendix C gives further details about the experimental setup and used baselines.

For our experiments, we run a varying number of tasks from the DeepMind Control Suite (Tassa et al., 2020) and report aggregated results over these tasks. Such aggregation is possible as the rewards in the DeepMind Control Suite are normalized, and all sequences are of equal length (1,000 steps). Thus the returns are normalized, and aggregation yields better performance estimates (Agarwal et al., 2021). Again following the suggestions of Agarwal et al. (2021), we report interquartile means while indicating 95% stratified bootstrap confidence intervals by shaded areas. These metrics are computed using the provided library[3]. We base our conclusions on those aggregated results. Unless noted otherwise, we use 10 seeds for each agent-environment pair, train for 1 million environment steps, and approximate the expected return using 10 rollouts. Appendix D provides reward curves for the individual tasks and additional quantitative results, such as box plots of their final performance.

4.1 Evaluation of the Effect of Epistemic Uncertainty on Different Smoothing Architectures

We start our evaluation by comparing the original *RSSM* with its extended smoothing version using a GRU with and without Monte Carlo Dropout (MCD), described in Section 2.3. For completeness, we also include a version of the original-*RSSM* with MCD to model epistemic uncertainty. For the *PlaNet*-agents, we evaluate the 6 tasks originally used in (Hafner et al., 2019). For the *Dreamer*-agents we use 8 tasks. Those are Cheetah Run, Walker Walk, Cartpole Swingup, Cup Catch, Reacher Easy, Hopper Hop, Pendulum Swingup, and Walker Run. As indicated by the results in Figure 4, the proper smoothing inference significantly deteriorates performance. Adding epistemic uncertainty in the form of MCD does, on average, neither affect the performance of the original *RSSM* nor the smoothing *RSSM*. These results underpin the argument that naive smoothing with the *RSSM* gives suboptimal performance. Additionally, they show that epistemic uncertainty in the form of Monte Carlo Dropout cannot serve as a remedy for the *RSSM*.

Next, we compare the *VRKN* to the *RSSM* using the same environments and also include a version of the *VRKN* without Monte Carlo Dropout (MCD), i.e., without epistemic uncertainty, dubbed *VRKN (no MCD)*. Figure 5 shows the aggregated results for both *PlaNet* and *Dreamer* agents. Those results demonstrate that matching the *RSSM's* performance is possible with a principled smoothing inference by explicitly modeling epistemic uncertainty and providing a more appropriate inductive bias. Additionally, we find the *VRKN* tends to reach a given performance with fewer environment interactions, especially for the *Dreamer*-agents.

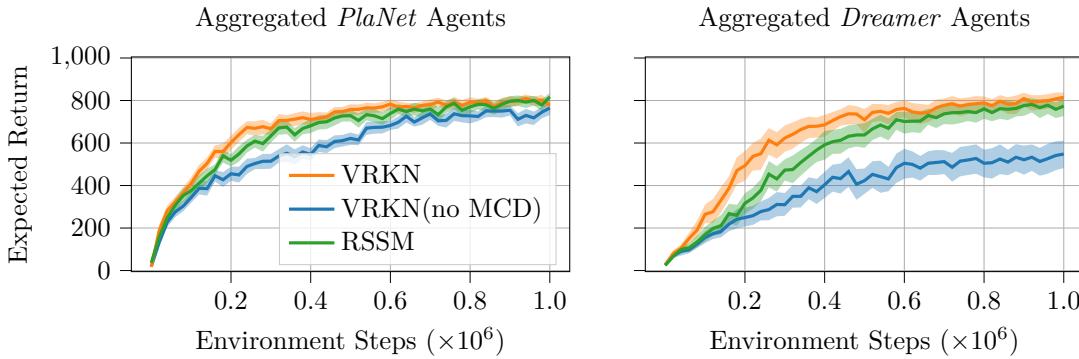[3]rliable: `https://github.com/google-research/rliable`

Figure 5: Comparison of *VRKN* and *RSSM* based *PlaNet* and *Dreamer* agents on standard DeepMind Control Suite tasks. Note that we use different tasks for *PlaNet* and *Dreamer*-based agents. Thus the left and right plots are not directly comparable. The *VRKN* without epistemic uncertainty (*VRKN (no MCD)*) cannot compete with the *RSSM*-agents, especially using the more involved *Dreamer*-based agents. Yet, the *VRKN* profits from the epistemic uncertainty, and closes the performance gap to the *RSSM* and even shows a tendency to be more sample efficient.

Together, the results from Figure 4 and Figure 5 emphasize the importance of regularization for model-based RL. This regularization can be either implicitly by suboptimal inference or explicitly by capturing epistemic uncertainty. Additionally, they indicate that epistemic uncertainty alone is insufficient for approaches using a correct smoothing inference. Yet, the *VRKN's* appropriate inductive bias makes the more principled approach of combining proper inference with explicit epistemic uncertainty feasible.

4.2 Evaluation on Tasks where Aleatoric Uncertainty Matters

The standard versions of the Deep Mind Control Suite Tasks have a deterministic simulation and rendering process. Thus, their aleatoric uncertainty is low. To better analyze the approaches' capabilities to capture and handle aleatoric uncertainty, we design tasks where doing so is necessary. To this end, we modify the Cheetah Run, Walker Walk, Cartpole Swingup, and Cup Catch tasks. First, we introduce transition noise by adding Gaussian noise to the actions before execution. We added noise with a standard deviation of 0.2 for Cheetah Run and Walker Walk and 0.3 for Cartpole Swingup and Cup Catch. Note that valid actions are between -1 and 1 for all tasks. Second, we modify the observations to contain only partial information, are missing for several time steps, or are available in different modalities at different frequencies. For details, we refer to the individual experiments below.

We use these tasks to study the effects of appropriately capturing aleatoric uncertainty in tasks where this form of uncertainty matters. We compare *VRKN*-based and the *RSSM*-based *Dreamer* agents and find that precise estimation of the aleatoric uncertainty makes a difference. Contrary to the original tasks, where *RSSM* and *VRKN*-based agents performed similarly, agents building on the *VRKN* outperform their *RSSM*-based counterparts in all considered scenarios.

4.2.1 Partial Observability through Occlusions

In a first approach to include observation uncertainty, we render two types of occlusions over the images, i.e., discs and walls. See Figure 6 for an explanation and some examples. Due to these occlusions, the individual observations have varying amounts of relevant information. Thus, the models need to correctly capture uncertainties in the system, allowing them to trade off information from the prior belief and current observation. For training, we use masked reconstruction, i.e., only non-occluded pixels contribute to the reconstruction loss[4]. We also consider a baseline where we train the model solely to reconstruct the reward to show that the approaches can still extract information from the highly occluded observations. Figure 7

---

[4]We want to emphasize that we do not consider the availability of such loss masks a realistic scenario but see the task as a reasonable benchmark to evaluate the models' capabilities to cope with uncertainties.
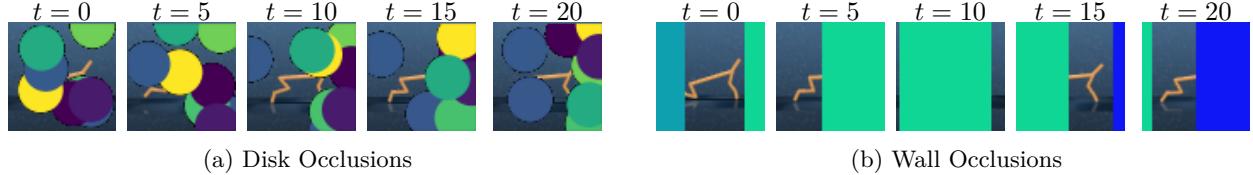
(a) Disk Occlusions

(b) Wall Occlusions

Figure 6: We introduce two types of occlusions to induce partial observability. **(a) Disk Occlusion:** Slow-moving disks float through the image and bounce off its walls. **(b)Wall Occlusions:** Walls slide over the image from right to left at a constant speed. Their width is sampled randomly between half the image width and the image width. In both cases, the models have to accurately estimate which parts of the system are visible and which are not. Yet, the wall-based occlusions are more correlated over time and require memorization and prediction over longer time periods.
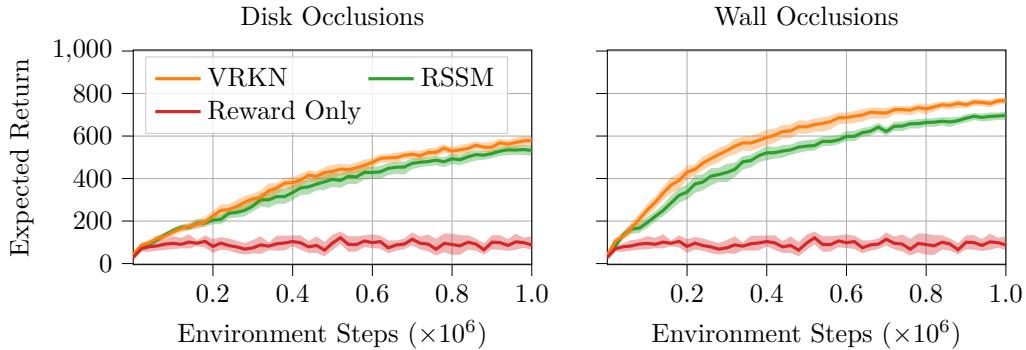
Figure 7: Aggregated results for the partial observability experiments with both occlusion types. For the experiments, except for the reward-only baseline, we used 20 seeds per task. Both approaches clearly perform better than the reward-only baseline, showing that they can extract useful information from the occluded images. Yet, especially in the wall-occlusion task, the *VRKN*-based agents outperform the *RSSM*-based agents. They do not only achieve a higher reward but also converge faster. Especially in the wall occlusion task, it is insufficient to only extract information from the occluded images, but a reasonable belief also needs to be sustained over time.

shows the results of the comparison. Under the heavy occlusions considered here, the *VRKN* performs significantly better than the *RSSM*. In particular for the wall occlusions, the *VRKN*-based agents achieve a higher reward using fewer environment interactions. The wall occlusions are more correlated, i.e., occluded parts in one image are more likely also occluded in the previous and next images. Thus, they test the approaches' capability to not only form a reasonable belief but also to propagate it for multiple time steps.

Additionally, we qualitatively compare images reconstructed from posterior beliefs of both approaches to gain further insights into the quality of the belief state. Figure 8 shows some of those reconstructions for the Cup Catch task, further images can be found in Appendix D.6. From these images, it appears that the *VRKN* better captures the actual system state and uncertainty and thus allows the model-based agent to achieve a higher reward. Yet, while the reconstructions are visually much better, we only observe a small increase in performance, which we attribute to *objective missmatch*.

4.2.2 Dealing with Missing Observations

Another common setting where estimating aleatoric uncertainty is important is missing observations. It requires the models to propagate a reasonable belief without information and update it if an observation is available. Additionally, if no observations are available for multiple time steps, the belief state gradually drifts away from the real state due to noise and model inaccuracies. Once a new observation arrives, the discrepancy between this observation and the belief has to be explained. Recall that, due to its inference assumptions, the *RSSM* must explain the discrepancy by the last transition and thus will overestimate the
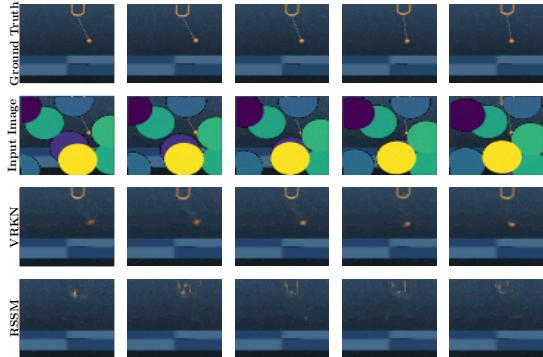
Figure 8: Exemplary sub-sequence of reconstructions, based on the model's posterior beliefs. The first row is the noise-free ground truth image, which the models never see. The second row is the model input, followed by the *VRKN* and the *RSSM* reconstructions. Even though the ball is partly visible in most images, the *RSSM* fails to reconstruct its position. The *VRKN* manages to do so and even provides a reasonable estimate for cup position. These results indicate the *VRKN's* improved ability to capture the system state in noisy scenarios.
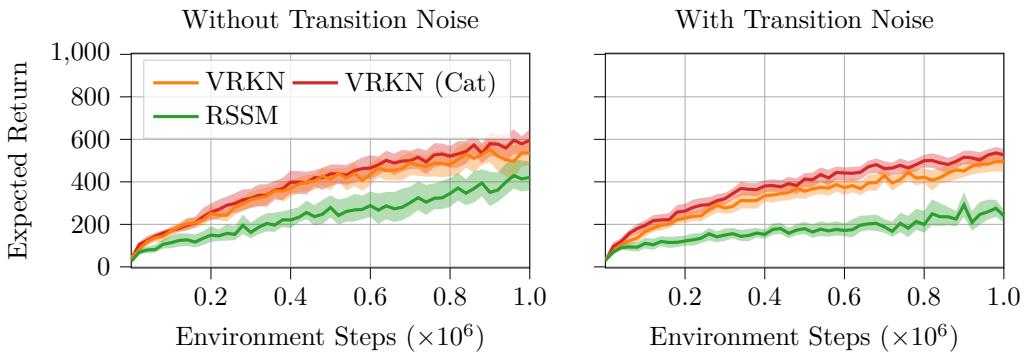
Figure 9: Aggregated results in the missing observations setting with and without transition noise. First, we see that the *VRKN* works equally well if we provide the information about which information are valid explicitly (*VRKN*) or if we provide it by concatenation (*VRKN (Cat)*). Second, the *RSSM* performs significantly worse then both both *VRKN* version. Especially if the system is subject to transition noise it fails to give good results.

aleatoric uncertainty even further. On the other hand, the *VRKN* with its smoothing inference can capture the drift of the belief state and evenly attribute the discrepancy to all transitions since the last observation. Thus the *VRKN* should be better equipped to solve such a task.

We consider a setting where we only provide every n-th image, where n is sampled uniformly between 4 and 8. We assume knowledge about whether the observation for a given time step is valid and feed that knowledge to the models as an additional input flag. For valid observation, the model receives the observation and a 1. For invalid observations, it receives a default value and a 0. The *RSSM* handles this flag by appending it to the encoder output[5] or the default value. The *VRKN* allows for two ways of handling the flag. First, we can again concatenate it to the observation before computing the latent observation and corresponding uncertainty estimate (*VRKN (Cat)*). Second, the *VRKNs* design allows us to provide the information more explicitly and the Kalman update step for invalid observations during inference. We evaluate with and without additional transition noise and show the results in Figure 9. Those results underpin the initial hypotheses that the *VRKN* is better equipped to learn in this setting and significantly outperforms the *RSSM*. The improvement is independent of how we provide information about missing information to the *VRKN* and, as expected, more significant with transition noise.

4.2.3 Fusing Information from Multiple Sensors at Different Frequencies

We extend the missing observations setting using proprioceptive information which is available at every time step. The exact form of the proprioceptive information is task-dependent. For example, for Cup Catch, we define the cup position as proprioceptive, but not the ball position, which has to be inferred from

---

[5]For the *RSSM* we refer to the convolution network processing the inputs as encoder, see Appendix C.3 for details.
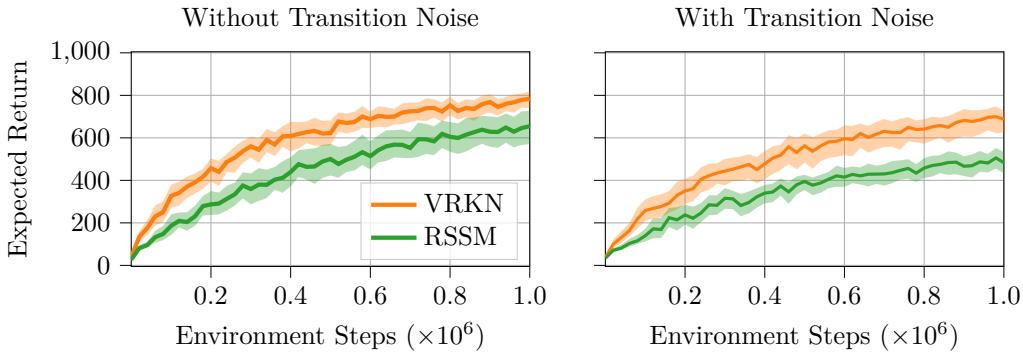
Figure 10: Aggregated results in the fusion setting with and without transition noise. When comparing to Figure 9 we see that both approaches are able to exploit the additional proprioceptive information and improve their performance. Yet, the *VRKN* seems to better exploit and accumulate the available information, as the resulting agents significantly outperform their *RSSM*-based counterparts.

images. Appendix C.4 provides an overview for all considered tasks. This experiment mimics a common robotics scenario where we have proprioceptive information about the robot at high frequencies but need to estimate the environment's state based on lower-frequency images. It tests the approaches' abilities to form reasonable state estimates from observations that arrive in different modalities and at varying frequencies. Here, the models need to trade off information encoded in the prior belief with the information available in both sensor sources. This trade off requires accurate estimates about the aleatoric uncertainty in both state and observations. For the fusion task, the *VRKN* can rely on the natural fusion mechanism described in Section 3. For the *RSSM*, we also use multiple encoder networks, decoders, and loss terms and concatenate the outputs of the encoders before forming the posterior belief. For details, see Appendix C.3.

As shown in Figure 10, the *VRKN* achieves a higher reward than the *RSSM*, especially in the setting with transition noise. This result again emphasizes the *VRKNs* capability to exploit all available information, appropriately capture the system's uncertainty, and form belief states that yield good performance.

5 Related Work

Recurrent State Space Models. While earlier works (Wahlström et al., 2015; Watter et al., 2015; Banijamali et al., 2018; Ha & Schmidhuber, 2018; Buesing et al., 2018) discussed and showed the feasibility of control using learned latent state space models, the work originally proposing the *RSSM* (Hafner et al., 2019) was the first to show that such approaches can achieve similar performance to model-free RL on pixel-based complex continuous control tasks while using significantly fewer environment interactions. Since then, Hafner et al. (2020) improved their approach using a parametric policy learned on imagined trajectories and categorical latent spaces (Hafner et al., 2021). These approaches gained interest in the model-based RL community and are empirically successful, yet, little attention has been paid to the underlying state space model itself, the assumptions it builds upon, and its parametrization.

State Space Models. The Machine Learning community extensively studied and used state space models (SSMs). Besides classical approaches using linear models (Shumway & Stoffer, 1982) and works using Gaussian Processes (Eleftheriadis et al., 2017; Doerr et al., 2018), most recent methods build on Neural Networks (NNs). The first class of NN-based models of particular relevance for this work embeds linear-Gaussian SSMs (LGSSM) into latent spaces (Watter et al., 2015; Karl et al., 2016; Fraccaro et al., 2017; Banijamali et al., 2018; Becker-Ehmck et al., 2019; Klushyn et al., 2021). These approaches assume actuated systems and learn using stochastic gradient variational Bayes (Kingma & Welling, 2013). Yet, non of these approaches were used to model or even control systems of the complexity considered by (Hafner et al., 2019) and here. They are not directly applicable to these scenarios for various reasons. First, they use full transition matrices and covariances, which prevents them from scaling to sufficiently high-dimensional latent spaces. (Karl et al., 2016; Becker-Ehmck et al., 2019) do not allow smoothing. (Fraccaro et al., 2017;

Klushyn et al., 2021) model the latent observations as random variables which are inferred jointly with the latent states and use constant observation uncertainty for the filtering in the latent space. This choice complicates inference and training and prevents principled usage of the observation uncertainty for filtering. Our parameterization of the LGSSM alleviates these issues by building on factorization assumptions which yield a scalable architecture. Further, it allows smoothing and principled usage of observation uncertainty during filtering by modeling the observations in latent space as deterministic. Finally, non of these approaches considered modeling epistemic uncertainty.

Another class of approaches directly uses NN-based, nonlinear parametrization for SSMs (Archer et al., 2015; Krishnan et al., 2015; Gu et al., 2015; Zheng et al., 2017; Krishnan et al., 2017; Yingzhen & Mandt, 2018; Schmidt & Hofmann, 2018; Naesseth et al., 2018; Moretti et al., 2019). Out of this class, *Structured Inference Networks (SINs)* (Krishnan et al., 2017) are the most relevant for our work. *SINs* build on the same variational objective as *VRKN*, yet without conditioning on actions. The smoothing-*RSSM* baseline introduced in Section 2.3 can be considered an instance of a *SIN*. Yet while it builds on the same loss and fundamental ideas, the underlying NN architecture is different.

Kalman Updates in Deep Latent Space. Haarnoja et al. (2016) first proposed using an encoder to extract uncertainty estimates from high-dimensional observations for filtering. They only learned the encoder while assuming the transition dynamics to be known. Becker et al. (2019) proposed an efficient factorization to additionally learn a high-dimensional, latent, locally-linear dynamics model. Shaj et al. (2020) extended this approach by introducing a principled form of action conditioning. While the *VRKN* builds on many of their design choices, there are also considerable differences. Those differences mainly concern the parametrization of the dynamics model and further simplifying the factorization assumptions. These changes are necessary to make the approaches scale to the complex control tasks considered in this work. Additionally, Haarnoja et al. (2016); Becker et al. (2019); Shaj et al. (2020) train using regression and do not learn a full generative model. Thus, they cannot produce the reasonable latent trajectories needed for model-based RL.

Epistemic Uncertainty for Model-Based RL. Ample work emphasises the importance of modeling epistemic uncertainty for model-based RL (Deisenroth & Rasmussen, 2011; Chua et al., 2018; Janner et al., 2019) and several authors equipped *RSSMs* with epistemic uncertainty. Okada et al. (2020) use an ensemble of *RSSMs* and showed improved results on modified versions of the Deep Mind Control Suite (Tassa et al., 2020) benchmarks. Sekar et al. (2020) also combine an ensemble with the *RSSM* but focus on exploration and generalization to unseen tasks. Yet, neither of these works questioned the assumptions underlying the *RSSM* or analyzed their effects on the learned models.

6 Conclusion

We analyzed the independence assumptions underlying *Recurrent State Space Models (RSSMs)* and found they are theoretically suboptimal. Yet, they implicitly regularize the model by causing an overestimated aleatoric uncertainty and are crucial to the *RSSMs* success in model-based RL. When trying to avoid this heuristic approach and use the correct assumptions while replacing the implicit regularization with a more explicit approach using epistemic uncertainty, we found a simple extension of the *RSSM* architecture is insufficient. Thus, we redesigned the model using well-understood and established components, providing a more appropriate inductive bias for smoothing. The resulting *Variational Recurrent Kalman Network (VRKN)* uses a latent linear Gaussian State Space Model (LGSSM) to address aleatoric uncertainty and Monte-Carlo Dropout to model epistemic uncertainty explicitly. Building on an LGSSM allows exact inference in the latent space using Kalman filtering and smoothing to obtain both smoothed and posterior belief states efficiently. While agents based on the *VRKN* and the *RSSM* perform similar on the standard DeepMind Control Suite (Tassa et al., 2020) benchmarks, the *VRKN*-based agents significantly outperform those using the *RSSM* on tasks where capturing uncertainties is more relevant. Additionally, the *VRKN* provides a natural approach to sensor fusion and outperforms the RSSM on tasks that require fusing sensor observations from several sensors at different frequencies.

Limitations. We showed that designing a state space model out of well-founded components that matches or improves the *RSSMs* performance is possible. This insight opens a path to improve them individually.

Yet, here we used simple instances of these components and have not yet further investigated how to improve them. Further, we have not investigated the interplay between the models and the controllers used on top of them but used the control approaches proposed in (Hafner et al., 2019) and (Hafner et al., 2020) with default parameters. Due to the intricate interplay between model learning and using the resulting controller for data collection, it is reasonable to rethink the design of the controller when changing the model.

Acknowledgments

References

Rishabh Agarwal, Max Schwarzer, Pablo Samuel Castro, Aaron C Courville, and Marc Bellemare. Deep reinforcement learning at the edge of the statistical precipice. *Advances in neural information processing systems*, 34:29304–29320, 2021.

Evan Archer, Il Memming Park, Lars Buesing, John Cunningham, and Liam Paninski. Black box variational inference for state space models. *arXiv preprint arXiv:1511.07367*, 2015.

Ershad Banijamali, Rui Shu, Hung Bui, Ali Ghodsi, et al. Robust locally-linear controllable embedding. In *International Conference on Artificial Intelligence and Statistics*, pp. 1751–1759. PMLR, 2018.

Philipp Becker, Harit Pandya, Gregor Gebhardt, Cheng Zhao, C James Taylor, and Gerhard Neumann. Recurrent kalman networks: Factorized inference in high-dimensional deep feature spaces. In *International Conference on Machine Learning*, pp. 544–552, 2019.

Philip Becker-Ehmck, Jan Peters, and Patrick Van Der Smagt. Switching linear dynamics for variational Bayes filtering. In Kamalika Chaudhuri and Ruslan Salakhutdinov (eds.), *Proceedings of the 36th International Conference on Machine Learning*, volume 97 of *Proceedings of Machine Learning Research*, pp. 553–562. PMLR, 09–15 Jun 2019.

Lars Buesing, Theophane Weber, Sébastien Racaniere, SM Eslami, Danilo Rezende, David P Reichert, Fabio Viola, Frederic Besse, Karol Gregor, Demis Hassabis, et al. Learning and querying fast generative models for reinforcement learning. *arXiv preprint arXiv:1802.03006*, 2018.

Kyunghyun Cho, Bart Van Merriënboer, Dzmitry Bahdanau, and Yoshua Bengio. On the properties of neural machine translation: Encoder-decoder approaches. *arXiv preprint arXiv:1409.1259*, 2014.

Kurtland Chua, Roberto Calandra, Rowan McAllister, and Sergey Levine. Deep reinforcement learning in a handful of trials using probabilistic dynamics models. *Advances in Neural Information Processing Systems*, 31, 2018.

Marc Deisenroth and Carl E Rasmussen. Pilco: A model-based and data-efficient approach to policy search. In *Proceedings of the 28th International Conference on machine learning (ICML-11)*, pp. 465–472. Citeseer, 2011.

Andreas Doerr, Christian Daniel, Martin Schiegg, Nguyen-Tuong Duy, Stefan Schaal, Marc Toussaint, and Trimpe Sebastian. Probabilistic recurrent state-space models. In *International Conference on Machine Learning*, pp. 1280–1289. PMLR, 2018.

Stefanos Eleftheriadis, Tom Nicholson, Marc Peter Deisenroth, and James Hensman. Identification of gaussian process state space models. In *NIPS*, pp. 5309–5319, 2017.

Marco Fraccaro, Simon Kamronn, Ulrich Paquet, and Ole Winther. A disentangled recognition and nonlinear dynamics model for unsupervised learning. In *Advances in Neural Information Processing Systems*, pp. 3601–3610, 2017.

Yarin Gal and Zoubin Ghahramani. Dropout as a bayesian approximation: Representing model uncertainty in deep learning. In *international conference on machine learning*, pp. 1050–1059. PMLR, 2016.

S Gu, Z Ghahramani, and RE Turner. Neural adaptive sequential monte carlo. *Advances in Neural Information Processing Systems*, 2015:2629–2637, 2015.

Fredrik Gustafsson. *Statistical sensor fusion*. Studentlitteratur, 2010.

David Ha and Jürgen Schmidhuber. World models. *arXiv preprint arXiv:1803.10122*, 2018.

Tuomas Haarnoja, Anurag Ajay, Sergey Levine, and Pieter Abbeel. Backprop kf: learning discriminative deterministic state estimators. In *Proceedings of the 30th International Conference on Neural Information Processing Systems*, pp. 4383–4391, 2016.

Danijar Hafner, Timothy Lillicrap, Ian Fischer, Ruben Villegas, David Ha, Honglak Lee, and James Davidson. Learning latent dynamics for planning from pixels. In *International Conference on Machine Learning*, pp. 2555–2565. PMLR, 2019.

Danijar Hafner, Timothy Lillicrap, Jimmy Ba, and Mohammad Norouzi. Dream to control: Learning behaviors by latent imagination. In *International Conference on Learning Representations*, 2020.

Danijar Hafner, Timothy P Lillicrap, Mohammad Norouzi, and Jimmy Ba. Mastering atari with discrete world models. In *International Conference on Learning Representations*, 2021. URL `https://openreview.net/forum?id=0oabwyZbOu`.

Sepp Hochreiter and Jürgen Schmidhuber. Long short-term memory. *Neural computation*, 9(8):1735–1780, 1997.

Eyke Hüllermeier and Willem Waegeman. Aleatoric and epistemic uncertainty in machine learning: An introduction to concepts and methods. *Machine Learning*, 110(3):457–506, 2021.

Michael Janner, Justin Fu, Marvin Zhang, and Sergey Levine. When to trust your model: Model-based policy optimization. *Advances in Neural Information Processing Systems*, 32:12519–12530, 2019.

AH Jazwinski. *Stochastic processes and filtering theory*. ACADEMIC PRESS, INC., 1970.

Rudolph Emil Kalman. A new approach to linear filtering and prediction problems. *Journal of basic Engineering*, 82(1):35–45, 1960.

Maximilian Karl, Maximilian Soelch, Justin Bayer, and Patrick van der Smagt. Deep variational bayes filters: Unsupervised learning of state space models from raw data. *arXiv preprint arXiv:1605.06432*, 2016.

Diederik P Kingma and Jimmy Ba. Adam: A method for stochastic optimization. In *ICLR (Poster)*, 2015.

Diederik P Kingma and Max Welling. Auto-encoding variational bayes. *arXiv preprint arXiv:1312.6114*, 2013.

Alexej Klushyn, Richard Kurle, Maximilian Soelch, Botond Cseke, and Patrick van der Smagt. Latent matters: Learning deep state-space models. *Advances in Neural Information Processing Systems*, 34, 2021.

Rahul Krishnan, Uri Shalit, and David Sontag. Structured inference networks for nonlinear state space models. In *Proceedings of the AAAI Conference on Artificial Intelligence*, volume 31, 2017.

Rahul G Krishnan, Uri Shalit, and David Sontag. Deep kalman filters. *arXiv preprint arXiv:1511.05121*, 2015.

Nathan Lambert, Brandon Amos, Omry Yadan, and Roberto Calandra. Objective mismatch in model-based reinforcement learning. *Proceedings of Machine Learning Research vol*, 120:1–15, 2020.

Yuping Luo, Huazhe Xu, Yuanzhi Li, Yuandong Tian, Trevor Darrell, and Tengyu Ma. Algorithmic framework for model-based deep reinforcement learning with theoretical guarantees. In *International Conference on Learning Representations*, 2019.

Michael Lutter, Leonard Hasenclever, Arunkumar Byravan, Gabriel Dulac-Arnold, Piotr Trochim, Nicolas Heess, Josh Merel, and Yuval Tassa. Learning dynamics models for model predictive agents. *arXiv preprint arXiv:2109.14311*, 2021.

Antonio Moretti, Zizhao Wang, Luhuan Wu, and Itsik Pe'er. Smoothing nonlinear variational objectives with sequential monte carlo, 2019.

Kevin P Murphy. *Machine learning: a probabilistic perspective*. MIT press, 2012.

Christian Naesseth, Scott Linderman, Rajesh Ranganath, and David Blei. Variational sequential monte carlo. In *International Conference on Artificial Intelligence and Statistics*, pp. 968–977. PMLR, 2018.

Masashi Okada, Norio Kosaka, and Tadahiro Taniguchi. Planet of the bayesians: Reconsidering and improving deep planning network by incorporating bayesian inference. *arXiv preprint arXiv:2003.00370*, 2020.

Herbert E Rauch, F Tung, and Charlotte T Striebel. Maximum likelihood estimates of linear dynamic systems. *AIAA journal*, 3(8):1445–1450, 1965.

Florian Schmidt and Thomas Hofmann. Deep state space models for unconditional word generation. *Advances in Neural Information Processing Systems 31*, 31:6158–6168, 2018.

Ramanan Sekar, Oleh Rybkin, Kostas Daniilidis, Pieter Abbeel, Danijar Hafner, and Deepak Pathak. Planning to explore via self-supervised world models. In *International Conference on Machine Learning*, pp. 8583–8592. PMLR, 2020.

Vaisakh Shaj, Philipp Becker, Dieter Buchler, Harit Pandya, Niels van Duijkeren, C James Taylor, Marc Hanheide, and Gerhard Neumann. Action-conditional recurrent kalman networks for forward and inverse dynamics learning. *Conference on Robot Learning*, 2020.

Robert H Shumway and David S Stoffer. An approach to time series smoothing and forecasting using the em algorithm. *Journal of time series analysis*, 3(4):253–264, 1982.

Kihyuk Sohn, Honglak Lee, and Xinchen Yan. Learning structured output representation using deep conditional generative models. *Advances in neural information processing systems*, 28:3483–3491, 2015.

Yuval Tassa, Yotam Doron, Alistair Muldal, Tom Erez, Yazhe Li, Diego de Las Casas, David Budden, Abbas Abdolmaleki, Josh Merel, Andrew Lefrancq, et al. Deepmind control suite. *arXiv preprint arXiv:1801.00690*, 2018.

Yuval Tassa, Saran Tunyasuvunakool, Alistair Muldal, Yotam Doron, Siqi Liu, Steven Bohez, Josh Merel, Tom Erez, Timothy Lillicrap, and Nicolas Heess. dm_control: Software and tasks for continuous control, 2020.

Michael Volpp, Fabian Flürenbrock, Lukas Grossberger, Christian Daniel, and Gerhard Neumann. Bayesian context aggregation for neural processes. In *International Conference on Learning Representations*, 2021.

Niklas Wahlström, Thomas B Schön, and Marc Peter Deisenroth. From pixels to torques: Policy learning with deep dynamical models. *arXiv preprint arXiv:1502.02251*, 2015.

Manuel Watter, Jost Springenberg, Joschka Boedecker, and Martin Riedmiller. Embed to control: A locally linear latent dynamics model for control from raw images. In *Advances in neural information processing systems*, pp. 2746–2754, 2015.

Li Yingzhen and Stephan Mandt. Disentangled sequential autoencoder. In Jennifer Dy and Andreas Krause (eds.), *Proceedings of the 35th International Conference on Machine Learning*, volume 80 of *Proceedings of Machine Learning Research*, pp. 5670–5679. PMLR, 10–15 Jul 2018.

Xun Zheng, Manzil Zaheer, Amr Ahmed, Yuan Wang, Eric P Xing, and Alexander J Smola. State space lstm models with particle mcmc inference. *arXiv preprint arXiv:1711.11179*, 2017.

A Derivations

For the derivations, we omit the subscripts for the generative and inference model $\boldsymbol{\theta}$ and $\boldsymbol{\phi}$ as the derivations are independent of those.

A.1 Lower Bound Objective

Derivation of the general ELBO objective (Equation 1)

$$
\begin{aligned}
\log p(\mathbf{o}_{\leq T}|\mathbf{a}_{\leq T}) &= \log \frac{p(\mathbf{o}_{\leq T}, \mathbf{z}_{\leq T}|\mathbf{a}_{\leq T})}{p(\mathbf{z}_{\leq T}|\mathbf{o}_{\leq T}, \mathbf{a}_{\leq T})} \\
&= \mathbb{E}_{q(\mathbf{z}_{\leq T}|\mathbf{o}_{\leq T}, \mathbf{a}_{\leq T})} \left[\log \frac{p(\mathbf{o}_{\leq T}|\mathbf{z}_{\leq T}, \mathbf{a}_{\leq T})p(\mathbf{z}_{\leq T}|\mathbf{a}_{\leq T})}{p(\mathbf{z}_{\leq T}|\mathbf{o}_{\leq T}, \mathbf{a}_{\leq T})} + \log \frac{q(\mathbf{z}_{\leq T}|\mathbf{o}_{\leq T}, \mathbf{a}_{\leq T})}{q(\mathbf{z}_{\leq T}|\mathbf{o}_{\leq T}, \mathbf{a}_{\leq T})} \right] \\
&= \underbrace{\mathbb{E}_{q(\mathbf{z}_{\leq T}|\mathbf{o}_{\leq T}, \mathbf{a}_{\leq T})} \left[\log p(\mathbf{o}_{\leq T}|\mathbf{z}_{\leq T}, \mathbf{a}_{\leq T}) \right] - \mathrm{KL}\left[q(\mathbf{z}_{\leq T}|\mathbf{o}_{\leq T}, \mathbf{a}_{\leq T}) \parallel p(\mathbf{z}_{\leq T},|\mathbf{a}_{\leq T}) \right]}_{\text{ELBO}} \\
&\quad + \underbrace{\mathrm{KL}\left[q(\mathbf{z}_{\leq T}|\mathbf{o}_{\leq T}, \mathbf{a}_{\leq T}) \parallel p(\mathbf{z}_{\leq T}|\mathbf{o}_{\leq T}, \mathbf{a}_{\leq T}) \right]}_{\text{KL term}(\geq 0)} \\
&= \underbrace{\mathbb{E}_{q(\mathbf{z}_{\leq T}|\mathbf{o}_{\leq T}, \mathbf{a}_{\leq T})} \left[\log \frac{p(\mathbf{o}_{\leq T}, \mathbf{z}_{\leq T}|\mathbf{a}_{\leq T})}{q(\mathbf{z}_{\leq T}|\mathbf{o}_{\leq T}, \mathbf{a}_{\leq T})} \right]}_{\text{ELBO}} + \underbrace{\mathrm{KL}\left[q(\mathbf{z}_{\leq T}|\mathbf{o}_{\leq T}, \mathbf{a}_{\leq T}) \parallel p(\mathbf{z}_{\leq T}|\mathbf{o}_{\leq T}, \mathbf{a}_{\leq T}) \right]}_{\text{KL term}(\geq 0)}.
\end{aligned}
$$

Before we derive the decomposition of the KL term under the *RSSM*-assumptions (Equation 2) and the lower bound under the *SSM*-assumptions (Equation 4), let us restate the independece assumptions. For all approaches, the joint generative model factorizes as (cf. the graphical model in Figure 1a)

$$
p(\mathbf{o}_{\leq T}, \mathbf{z}_{\leq T}|\mathbf{a}_{\leq T}) = p(\mathbf{z}_0) \prod_{t=1}^{T} p(\mathbf{z}_t|\mathbf{z}_{t-1}, \mathbf{a}_{t-1}) \prod_{t=0}^{T} p(\mathbf{o}_t|\mathbf{z}_t).
$$

The same independence assumptions imply the following decomposition for the conditional distribution over latent states given observations and actions $p(\mathbf{z}_{\leq T}|\mathbf{o}_{\leq T}, \mathbf{a}_{\leq T})$

$$
p(\mathbf{z}_{\leq T}|\mathbf{o}_{\leq T}, \mathbf{a}_{\leq T}) = p(\mathbf{z}_0|\mathbf{o}_{\leq T}, \mathbf{a}_{\leq T}) \prod_{t=1}^{T} p(\mathbf{z}_t|\mathbf{z}_{\leq t-1}, \mathbf{o}_{\leq T}, \mathbf{a}_{\leq T}) = p(\mathbf{z}_0|\mathbf{o}_{\leq T}, \mathbf{a}_{\leq T}) \prod_{t=1}^{T} p(\mathbf{z}_t|\mathbf{z}_{t-1}, \mathbf{o}_{\geq t}, \mathbf{a}_{\geq t-1}).
$$

Thus, when using the same assumptions for the variational inference distribution $q(\mathbf{z}_{\leq T}|\mathbf{o}_{\leq T}, \mathbf{a}_{\leq T})$, it also factorizes as

$$
q(\mathbf{z}_{\leq T}|\mathbf{o}_{\leq T}, \mathbf{a}_{\leq T}) = q(\mathbf{z}_0|\mathbf{o}_{\leq T}, \mathbf{a}_{\leq T}) \prod_{t=1}^{T} q(\mathbf{z}_t|\mathbf{z}_{t-1}, \mathbf{o}_{\geq t}, \mathbf{a}_{\geq t-1}).
$$

Contrary to that, as introduced by (Hafner et al., 2019), the *RSSM*'s joint variational distribution factorizes as (cf. the graphical model in Figure 1b)

$$
q(\mathbf{o}_{\leq T}, \mathbf{z}_{\leq T}|\mathbf{a}_{\leq T}) = q(\mathbf{z}_0|\mathbf{o}_0) \prod_{t=1}^{T} q(\mathbf{z}_t|\mathbf{z}_{t-1}, \mathbf{o}_t, \mathbf{a}_{t-1}) \prod_{t=0}^{T} q(\mathbf{o}_t).
$$

Thus the variational inference distribution is given by

$$
q(\mathbf{z}_{\leq T}|\mathbf{o}_{\leq T}, \mathbf{a}_{\leq T}) = \frac{q(\mathbf{o}_{\leq T}, \mathbf{z}_{\leq T}|\mathbf{a}_{\leq T})}{q(\mathbf{o}_{\leq T})} = q(\mathbf{z}_0|\mathbf{o}_0) \prod_{t=1}^{T} q(\mathbf{z}_t|\mathbf{z}_{t-1}, \mathbf{o}_t, \mathbf{a}_{t-1}).
$$

Let us now consider the KL term of the lower bound decomposition (Equation 1) when using the generative assumptions for p and the *RSSM*'s inference assumptions for q. We get Equation 2:

$$\mathrm{KL}\left(q(\mathbf{z}_{\leq T}|\mathbf{o}_{\leq T}, \mathbf{a}_{\leq T})||p(\mathbf{z}_{\leq T}|\mathbf{o}_{\leq T}, \mathbf{a}_{\leq T})\right)$$

$$= \int q(\mathbf{z}_0|\mathbf{o}_0)\prod_{t=1}^{T} q(\mathbf{z}_t|\mathbf{z}_{t-1}, \mathbf{o}_t, \mathbf{a}_{t-1})\left(\sum_{t=1}^{T}\log\frac{q(\mathbf{z}_t|\mathbf{z}_{t-1}, \mathbf{o}_t, \mathbf{a}_{t-1})}{p(\mathbf{z}_t|\mathbf{z}_{t-1}, \mathbf{o}_{\geq t}, \mathbf{a}_{\geq t-1})}\right)d\mathbf{z}_{\leq T}$$

$$= \sum_{t=1}^{T}\int\left(q(\mathbf{z}_0|\mathbf{o}_0)\prod_{t=1}^{T} q(\mathbf{z}_t|\mathbf{z}_{t-1}, \mathbf{o}_{\geq t}, \mathbf{a}_{\geq t-1})\right)\log\frac{q(\mathbf{z}_t|\mathbf{z}_{t-1}, \mathbf{o}_t, \mathbf{a}_{t-1})}{p(\mathbf{z}_t|\mathbf{z}_{t-1}, \mathbf{o}_{\geq t}, \mathbf{a}_{\geq t-1})}d\mathbf{z}_{\leq T}$$

$$= \sum_{t=0}^{T}\int\underbrace{\prod_{k=t+1}^{T} q(\mathbf{z}_k|\mathbf{z}_{k-1}, \mathbf{o}_k, \mathbf{a}_{k-1})d\mathbf{z}_k}_{=1}\underbrace{q(\mathbf{z}_0|\mathbf{o}_0)\prod_{k=1}^{t-2} q(\mathbf{z}_{k+1}|\mathbf{z}_k, \mathbf{o}_{k+1}, \mathbf{a}_k)d\mathbf{z}_k}_{q(\mathbf{z}_{t-1}|\mathbf{o}_{t-1}, \mathbf{a}_{t-2})}$$

$$\underbrace{q(\mathbf{z}_t|\mathbf{z}_{t-1}, \mathbf{o}_t, \mathbf{a}_{t-1})\log\frac{q(\mathbf{z}_t|\mathbf{z}_{t-1}, \mathbf{o}_t, \mathbf{a}_{t-1})}{p(\mathbf{z}_t|\mathbf{z}_{t-1}, \mathbf{o}_{\geq t}, \mathbf{a}_{\geq t-1})}d\mathbf{z}_t\, d\mathbf{z}_{t-1}}_{\mathrm{KL}\left(q(\mathbf{z}_t|\mathbf{z}_{t-1}, \mathbf{o}_t, \mathbf{a}_{t-1})||p(\mathbf{z}_t|\mathbf{z}_{t-1}, \mathbf{o}_{\geq t}, \mathbf{a}_{\geq t-1})\right)}$$

$$= \sum_{t=0}^{T}\mathbb{E}_{q(\mathbf{z}_{t-1}|\mathbf{o}_{\leq t-1}, \mathbf{a}_{\leq t-2})}\left[\mathrm{KL}\left[q(\mathbf{z}_t|\mathbf{z}_{t-1}, \mathbf{o}_t, \mathbf{a}_{t-1}) \,\|\, p(\mathbf{z}_t|\mathbf{z}_{t-1}, \mathbf{o}_{\geq t}, \mathbf{a}_{\geq t-1})\right]\right].$$

Plugging the same assumptions into the ELBO part of Equation 1 gives the *RSSM* objective already derived by Hafner et al. (2019) (Equation 3).

To derive our objective (Equation 4) we instead use the generative assumptions for both the generative model as well as the inference model. Again starting from the ELBO part of Equation 1, we get

$$\mathbb{E}_{q(\mathbf{z}_{\leq T}|\mathbf{o}_{\leq T}, \mathbf{a}_{\leq T})}\left[\log p(\mathbf{o}_{\leq T}|\mathbf{z}_{\leq T})\right] - \mathrm{KL}\left(q(\mathbf{z}_{\leq T}|\mathbf{o}_{\leq T}, \mathbf{a}_{\leq T})||p(\mathbf{z}_{\leq T}|\mathbf{a}_{\leq T})\right)$$

$$= \int\left(q(\mathbf{z}_0|\mathbf{o}_{\leq T}, \mathbf{a}_{\leq T})\prod_{t=1}^{T} q(\mathbf{z}_t|\mathbf{z}_{t-1}, \mathbf{a}_{\geq t-1}, \mathbf{o}_{\geq t})\right)\sum_{t=0}^{T}\log p(\mathbf{o}_t|\mathbf{z}_t)d\mathbf{z}_{\leq t}$$

$$- \int q(\mathbf{z}_0|\mathbf{o}_{\leq T}, \mathbf{a}_{\leq T})\prod_{t=1}^{T} q(\mathbf{z}_t|\mathbf{z}_{t-1}, \mathbf{a}_{\geq t-1}, \mathbf{o}_{\geq t})\left(\sum_{t=1}^{T}\log\frac{q(\mathbf{z}_t|\mathbf{z}_{t-1}, \mathbf{a}_{\geq t-1}, \mathbf{o}_{\geq t})}{p(\mathbf{z}_t|\mathbf{z}_{t-1}, \mathbf{a}_{t-1})}\right)d\mathbf{z}_{\leq T}$$

$$= \sum_{t=0}^{T}\int\left(q(\mathbf{z}_0|\mathbf{o}_{\leq T}, \mathbf{a}_{\leq T})\prod_{t=1}^{T} q(\mathbf{z}_t|\mathbf{z}_{t-1}, \mathbf{a}_{\geq t-1}, \mathbf{o}_{\geq t})\right)\log p(\mathbf{o}_t|\mathbf{z}_t)d\mathbf{z}_{\leq t}$$

$$- \sum_{t=1}^{T}\int\left(q(\mathbf{z}_0|\mathbf{o}_{\leq T}, \mathbf{a}_{\leq T})\prod_{t=1}^{T} q(\mathbf{z}_t|\mathbf{z}_{t-1}, \mathbf{a}_{\geq t-1}, \mathbf{o}_{\geq t})\right)\log\frac{q(\mathbf{z}_t|\mathbf{z}_{t-1}, \mathbf{a}_{\geq t-1}, \mathbf{o}_{\geq t})}{p(\mathbf{z}_t|\mathbf{z}_{t-1}, \mathbf{a}_{t-1})}d\mathbf{z}_{\leq T}$$

$$= \sum_{t=0}^{T}\int\underbrace{\prod_{k=t+1}^{T} q(\mathbf{z}_k|\mathbf{z}_{k-1}, \mathbf{a}_{\geq k-1}, \mathbf{o}_{\geq k})d\mathbf{z}_k}_{=1}$$

$$\underbrace{q(\mathbf{z}_0|\mathbf{o}_{\leq T}, \mathbf{a}_{\leq T})\prod_{k=1}^{t-1} q(\mathbf{z}_{k+1}|\mathbf{z}_k, \mathbf{a}_{\geq k}, \mathbf{o}_{\geq k+1})d\mathbf{z}_k\log p(\mathbf{o}_t|\mathbf{z}_t)d\mathbf{z}_t}_{q(\mathbf{z}_t|\mathbf{o}_{\leq T}, \mathbf{a}_{\leq T})}$$

$$- \sum_{t=0}^{T}\int\underbrace{\prod_{k=t+1}^{T} q(\mathbf{z}_k|\mathbf{z}_{k-1}, \mathbf{a}_{\geq k-1}, \mathbf{o}_{\geq k})d\mathbf{z}_k}_{=1}\underbrace{(q(\mathbf{z}_0|\mathbf{o}_{\leq T}, \mathbf{a}_{\leq T})\prod_{k=1}^{t-2} q(\mathbf{z}_{k+1}|\mathbf{z}_k, \mathbf{a}_{\geq k}, \mathbf{o}_{\geq k+1})d\mathbf{z}_k}_{q(\mathbf{z}_{t-1}|\mathbf{o}_{\leq T}, \mathbf{a}_{\leq T})}$$

$$\underbrace{q(\mathbf{z}_t|\mathbf{z}_{t-1}, \mathbf{a}_{\geq t-1}, \mathbf{o}_{\geq t},) \log \frac{q(\mathbf{z}_t|\mathbf{z}_{t-1}, \mathbf{a}_{\geq t-1}, \mathbf{o}_{\geq t})}{p(\mathbf{z}_t|\mathbf{z}_{t-1})} d\mathbf{z}_t \, d\mathbf{z}_{t-1}}_{\mathrm{KL}(q(\mathbf{z}_t|\mathbf{z}_{t-1}, \mathbf{a}_{\geq t-1}, \mathbf{o}_{\geq t})||p(\mathbf{z}_t|\mathbf{z}_{t-1}, \mathbf{a}_{t-1}))}$$

$$= \sum_{t=0}^{T} \mathbb{E}_{q(\mathbf{z}_t|\mathbf{o}_{\leq T}, \mathbf{a}_{\leq T})} \left[\log p(\mathbf{o}_t|\mathbf{z}_t)\right]$$

$$- \sum_{t=1}^{T} \mathbb{E}_{q(\mathbf{z}_{t-1}|\mathbf{o}_{\leq T}, \mathbf{a}_{\leq T})} \left[\mathrm{KL}\left[q(\mathbf{z}_t|\mathbf{z}_{t-1}, \mathbf{a}_{\geq t-1}, \mathbf{o}_{\geq t}) \parallel p(\mathbf{z}_t|\mathbf{z}_{t-1}, \mathbf{a}_{t-1})\right]\right].$$

A.2 Extended Backward Pass for Smoothed Dynamics

Here we derive an extended backward pass, i.e., given the forward priors and posteriors we are interested in the smoothed *state* $q(\mathbf{z}_{t-1}|\mathbf{o}_{\leq T}, \mathbf{a}_{\leq T})$ as well as the smoothed *dynamics* $q(\mathbf{z}_t|\mathbf{z}_{t-1}, \mathbf{a}_{\geq t-1}, \mathbf{o}_{\geq t})$. We can read off both these quantities from the joint smoothed estimate

$$q(\mathbf{z}_t, \mathbf{z}_{t-1}|\mathbf{o}_{\leq T}, \mathbf{a}_{\leq T}) = q(\mathbf{z}_t|\mathbf{z}_{t-1}, \mathbf{a}_{\geq t-1}, \mathbf{o}_{\geq t})q(\mathbf{z}_{t-1}|\mathbf{o}_{\leq T}, \mathbf{a}_{\leq T}).$$

This joint smoothed estimate can be computed using the identity

$$q(\mathbf{z}_t, \mathbf{z}_{t-1}|\mathbf{o}_{\leq T}, \mathbf{a}_{\leq T}) = q(\mathbf{z}_{t-1}|\mathbf{z}_t, \mathbf{o}_{\leq t-1}, \mathbf{a}_{\leq t-1})q(\mathbf{z}_t|\mathbf{o}_{\leq T}, \mathbf{a}_{\leq T})$$

$$= \frac{p(\mathbf{z}_t|\mathbf{z}_{t-1}, \mathbf{a}_{t-1})q(\mathbf{z}_{t-1}|\mathbf{o}_{\leq t-1}, \mathbf{a}_{\leq t-2})}{q(\mathbf{z}_t|\mathbf{o}_{\leq t-1}, \mathbf{a}_{\leq t-1})} q(\mathbf{z}_t|\mathbf{o}_{\leq T}, \mathbf{a}_{\leq T}). \tag{5}$$

All quantities in Equation 5 are available in closed form as the smoothed state-estimate $q(\mathbf{z}_t|\mathbf{o}_{\leq T}, \mathbf{a}_{\leq T})$ is computed during the previous iteration of the backward pass. To recursion starts with the last posterior which is equal to the smoothed estimate for $t = T$. We denote the parameters of the 4 distributions as follows

$$q(\mathbf{z}_t|\mathbf{o}_{\leq t-1}, \mathbf{a}_{\leq t-1}) = \mathcal{N}(\mathbf{z}_t|\boldsymbol{\mu}_t^-, \boldsymbol{\Sigma}_t^-), \quad q(\mathbf{z}_{t-1}|\mathbf{o}_{\leq t-1}, \mathbf{a}_{\leq t-2}) = \mathcal{N}(\mathbf{z}_{t-1}|\boldsymbol{\mu}_{t-1}^+, \boldsymbol{\Sigma}_{t-1}^+),$$

$$q(\mathbf{z}_t|\mathbf{o}_{\leq T}, \mathbf{a}_{\leq T}) = \mathcal{N}(\mathbf{z}_t|\boldsymbol{\mu}_t^s, \boldsymbol{\Sigma}_t^s) \text{ and } p(\mathbf{z}_t|\mathbf{z}_{t-1}, \mathbf{a}_{t-1}) = \mathcal{N}(\mathbf{z}_t|\mathbf{A}_{t-1}\mathbf{z}_{t-1} + \mathbf{B}_{t-1}\mathbf{a}_{t-1}, \boldsymbol{\Sigma}_{t-1}^{\mathrm{dyn}}).$$

Using Bayes rule we get

$$q(\mathbf{z}_{t-1}|\mathbf{z}_t, \mathbf{o}_{\leq t-1}, \mathbf{a}_{\leq t-1}) = \mathcal{N}(\boldsymbol{\mu}_{t-1}^+ + \mathbf{C}_{t-1}(\mathbf{z}_t - \underbrace{\mathbf{A}_{t-1}\boldsymbol{\mu}_{t-1}^+ + \mathbf{B}_{t-1}\mathbf{a}_{t-1}}_{\boldsymbol{\mu}_t^-}), (\mathbf{I} - \mathbf{C}_{t-1}\mathbf{A}_{t-1})\boldsymbol{\Sigma}_{t-1}^+)$$

with $\mathbf{C}_{t-1} = \boldsymbol{\Sigma}_{t-1}^+ \mathbf{A}_{t-1}^T \underbrace{(\mathbf{A}_{t-1}\boldsymbol{\Sigma}_{t-1}^+ \mathbf{A}_{t-1}^T + \boldsymbol{\Sigma}_{t-1}^{\mathrm{dyn}})}_{\boldsymbol{\Sigma}_t^-}^{-1} = \boldsymbol{\Sigma}_{t-1}^+ \mathbf{A}_{t-1}^T (\boldsymbol{\Sigma}_t^-)^{-1}$. Thus, the full "two-sliced" smoothed estimate is given by

$$q(\mathbf{z}_{t-1}, \mathbf{z}_t|\mathbf{o}_{\leq T}, \mathbf{a}_{\leq T}) = q(\mathbf{z}_{t-1}|\mathbf{z}_t, \mathbf{o}_{\leq t-1}, \mathbf{a}_{\leq t-1})q(\mathbf{z}_t|\mathbf{o}_{\leq T}, \mathbf{a}_{\leq T}) =$$

$$\mathcal{N}\left(\begin{pmatrix} \mathbf{z}_{t-1} \\ \mathbf{z}_t \end{pmatrix} \middle| \begin{pmatrix} \boldsymbol{\mu}_{t-1}^+ + \mathbf{C}_{t-1}(\boldsymbol{\mu}_t^s - \boldsymbol{\mu}_t^-) \\ \boldsymbol{\mu}_t^s \end{pmatrix}, \begin{pmatrix} (\mathbf{I} - \mathbf{C}_{t-1}\mathbf{A}_{t-1})\boldsymbol{\Sigma}_{t-1}^+ + \mathbf{C}_{t-1}\boldsymbol{\Sigma}_t^s\mathbf{C}_{t-1}^T & \mathbf{C}_{t-1}\boldsymbol{\Sigma}_t^s \\ \boldsymbol{\Sigma}_t^s\mathbf{C}_{t-1}^T & \boldsymbol{\Sigma}_t^s \end{pmatrix}\right)$$

$$= \mathcal{N}\left(\begin{pmatrix} \mathbf{z}_{t-1} \\ \mathbf{z}_t \end{pmatrix} \middle| \begin{pmatrix} \boldsymbol{\mu}_{t-1}^s \\ \boldsymbol{\mu}_t^s \end{pmatrix}, \begin{pmatrix} \boldsymbol{\Sigma}_{t-1}^s & \mathbf{C}_{t-1}\boldsymbol{\Sigma}_t^s \\ \boldsymbol{\Sigma}_t^s\mathbf{C}_{t-1}^T & \boldsymbol{\Sigma}_t^s \end{pmatrix}\right).$$

We can just read off the smoothed dynamics at time t from the joint above and get

$$q(\mathbf{z}_t|\mathbf{z}_{t-1}, \mathbf{a}_{\geq t-1}, \mathbf{o}_{\geq t})$$

$$= \mathcal{N}\left(\mathbf{z_t}|\boldsymbol{\mu}_t^s + \boldsymbol{\Sigma}_t^s\mathbf{C}_{t-1}^T(\boldsymbol{\Sigma}_{t-1}^s)^{-1}(\mathbf{z}_{t-1} - \boldsymbol{\mu}_{t-1}^s), \boldsymbol{\Sigma}_t^s - \boldsymbol{\Sigma}_t^s\mathbf{C}_{t-1}^T(\boldsymbol{\Sigma}_{t-1}^s)^{-1}\mathbf{C}_{t-1}\boldsymbol{\Sigma}_t^s\right).$$

We can also read off the smoothed state estimate at time $t-1$ and get the standard Rauch-Tung-Striebel backward recursion.

B Details on Introductory Example

Generative Model: The full generative linear-Gaussian State Space Model used to generate the data in Section 2.2 is given as

$$p(\mathbf{z}_0) = \mathcal{N}(\mathbf{0}, \mathbf{I}), \quad p(\mathbf{o}_t|\mathbf{z}_t) = \mathcal{N}(\mathbf{Iz}_t, 0.025\mathbf{I}), \quad p(\mathbf{z}_{t+1}|\mathbf{z}_t) = \mathcal{N}(\mathbf{Az_t}, 0.01\mathbf{I})$$

where

$$\mathbf{A} = \begin{pmatrix} 1.0 & 0.0 & 0.2 & 0.0 \\ 0.0 & 1.0 & 0.0 & 0.2 \\ -0.2 & 0.0 & 0.95 & 0.0 \\ 0.0 & -0.2 & 0.0 & 0.95 \end{pmatrix}.$$

We fix the initial state and observation model and only learn the dynamics model. The 16 entries of $\mathbf{A}$ are initialized randomly, sampled from $\mathcal{N}(0, 0.05)$. The transition covariance is isotropic, thus we only learn a scaling scalar initialized with 1. In the ground truth model, this factor is 0.01.

Inference for $\mathcal{L}_{\mathbf{rssm}}$ (Equation 3): Computing the optimal inference distribution under the *RSSM*-assumptions is not possible, even for this simple example. We thus parameterize it as $q(\mathbf{z}_{t+1}|\mathbf{z}_t, \mathbf{o}_t) = \mathcal{N}(\mathbf{C}_t\mathbf{z}_t + \mathbf{c}_t, \mathbf{\Sigma}_t^{\mathbf{c}})$, where $\mathbf{C}_t, \mathbf{c}_t, \mathbf{\Sigma}_t^{\mathbf{c}}$ are emitted by a small neural network given the observation and mean of the previous belief. This network is trained jointly with the generative model.

Inference for $\mathcal{L}_{\mathbf{ssm}}$ (Equation 4): For the state space assumptions, we can compute the optimal inference distribution in closed form using Kalman Smoothing. Thus we do not need an additional inference model ($\mathcal{L}_{\mathrm{ssm}}(\mathrm{CF})$ in Figure 2). Yet, to evaluate the general feasibility of the approach later used for the *Smoothing RSSM*, we also evaluate a NN-based inference distribution ($\mathcal{L}_{\mathrm{ssm}}(\mathrm{NN})$ in Figure 2). To this end, we use a GRU (Cho et al., 2014) to process the observations backward, extracting a latent representation of all future observations $\mathbf{o}_{\geq t}$ for each time step. We then feed this representation into the NN used for $\mathcal{L}_{\mathrm{rssm}}$ described above to get a NN emitting parameters for $q(\mathbf{z}_{t+1}|\mathbf{z}_t, \mathbf{o}_{\geq t})$.

Training: We train by maximizing the respective ELBOs using Adam(Kingma & Ba, 2015) with a learning rate of 0.005 on $1,000$ sequences with a length of 50 and a batch size of 50.

C Details on Experiment Setup, Baselines and Hyperparameters

We evaluate all variants of the *RSSM* and the *VRKN* in an experimental setup that closely follows (Hafner et al., 2019) as well as (Hafner et al., 2020) by exchanging the underlying model while keeping all other parts of the approach fix. We refer to the pseudo-code presented in those works for an overview of the training procedure.

C.1 Smoothing *RSSM*

The smoothing *RSSM* works very similar to the $\mathcal{L}_{\mathrm{ssm}}(\mathrm{CF})$ and uses a GRU (Cho et al., 2014) to accumulate information for all future time steps. This GRU is placed between the CNN which extracts the representation for the *RSSM* and the *RSSM* itself, as indicated by the dashed red line in Figure 11. It processes the CNN's output backward and extracts a latent representation of all future observations $\mathbf{o}_{\geq t}$ which is fed to the rest of the pipeline instead of the original CNN output. For online control, we only have $\mathbf{o}_t$ as all future information is unavailable. In this case, we only feed $\mathbf{o}_t$, together with the default initial memory value, through the GRU and give the output to the remaining pipeline.

C.2 *RSSM* with Monte Carlo Dropout

For the baseline with Bayesian treatment of the *RSSM*'s transition parameters, we combined the original *RSSM* with Monte Carlo Dropout (Gal & Ghahramani, 2016). Figure 11 provides an overview over the resulting architecture.
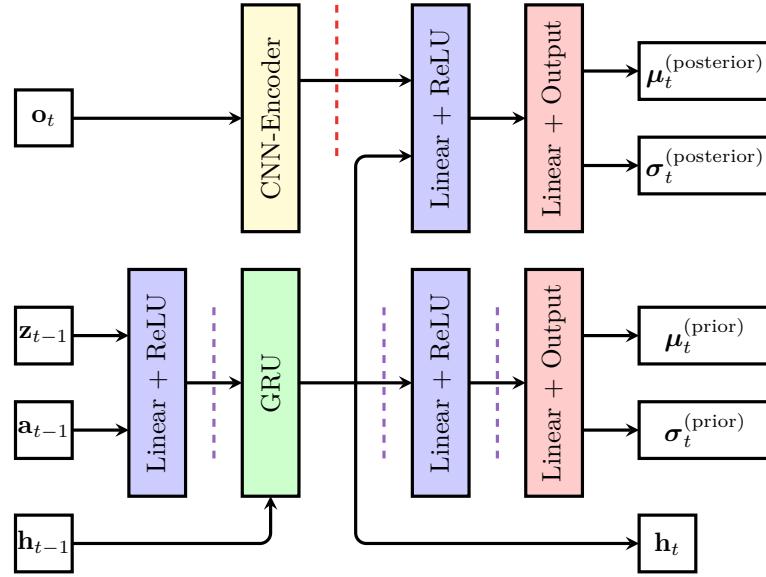
Figure 11: Overview over the dynamics and inference model of the *RSSM* with MC Dropout baseline. The general architecture is equivalent to that of the original *RSSM*, but we included Monte Carlo Dropout Layers at the locations indicated by the purple dashed lines. For preliminary experiments, we also included Dropout before the two linear layers in the computation path of the posterior but found that this decreases performance. The dashed red line indicates the position where the backward GRU is added for the smoothing version of the *RSSM*

.

Table 1: For the fusion experiment we split the standard observations of the environments into proprioceptive and non-proprioceptive as follows.

Environment	Proprioceptive	Non-Proprioceptive
cheetah run	Joints (`bthigh`, `bshin`, `bfoot`, `fthigh`, `fshin`, `ffoot`)	Global Position/Orientation: (`rootx`, `rooty`, `rootz`)
walker walk / run	orientation of links	height of center of mass above the ground
cartpole swingup	Cart position (`slider`)	Pole angle (`hinge`)
cup catch	Cup Position (`cup_x`, `cup_z`)	Ball Position(`ball_x`, `ball_z`)

C.3 Missing Observations and Fusion for *RSSM*.

For the experiments including missing observations, we concatenated the flag indicating the validity of the observation after the CNN-Encoder in Figure 11.

For fusion, we used several encoders, whose output we concatenate before passing it to the next linear layer (red dashed line in Figure 11). Like for the *VRKN*, we use a separate decoder an reconstruction loss term for all observations (c.f. Section 3.6)

C.4 Proprioceptive Joints in Fusion Tasks

Table 1 shows how we split the observations in into proprioceptive and non-proprioceptive information for the different environments. In all cases, we only provide positional information, no velocities.

C.5 Hyperparameters

Where applicable we reused the hyperparametes used in (Hafner et al., 2019) and (Hafner et al., 2020).

State Space Models. The exact parametrization of the *RSSM* (layer widths and activation functions) differs between (Hafner et al., 2019) and (Hafner et al., 2020) and we used the respective values for the respective agents. Both use a stochastic state size of 30 and a deterministic state size of 200.

For the *VRKN*, we used a common set of hyper-parameters for all experiments and a stochastic state size of 230, to match the total state size of the *RSSM* approaches. All layers, including the GRU cell, are of width 300 and all linear layers use ReLU activation. The transition matrix output of the transition network is transformed by the sigmoid-based transformation described in section 3, the offset output is unconstrained and the transition noise output is constrained by the sigmoid-based transformation, saturating at $0.001, 0.1$ while $f(0) = 0.01$.

For the Monte Carlo dropout-based approaches, we use a dropout rate of 0.1.

Encoder - Decoder. We used the convectional architectures originally introduced in (Ha & Schmidhuber, 2018) and later used in (Hafner et al., 2019; 2020). For the *VRKN* the encoder was augmented with a linear layer mapping to the latent observation and a linear layer + softplus for the uncertainty output.

For the reward decoder, we also followed (Hafner et al., 2019) and (Hafner et al., 2020) and used 2 layers of width 200 with ReLU activation for *PlaNet* experiments and 3 layers of width 300 with ELU activation for all the *Dreamer* experiments.

To encode low-dimensional proprioceptive observation in the fusion experiments we used an additional encoder network with 3 layers of width 300 with ELU activation.

Loss. Following the official implementation of (Hafner et al., 2019) we scaled the loss of the reward decoder by a factor of 10 for the *PlaNet* experiments. Ee also found this beneficial for the *VRKN*. While the *RSSM* (and all approaches based on the original parametrization) use a factor of 1 for Dreamer, we kept the factor of 10 for the *VRKN*-parametrization based approaches. In both cases, that led to better performance of the respective approaches. We used the 3-free nats trick used in (Hafner et al., 2019; 2020) to regularize the KL term for all experiments and approaches.
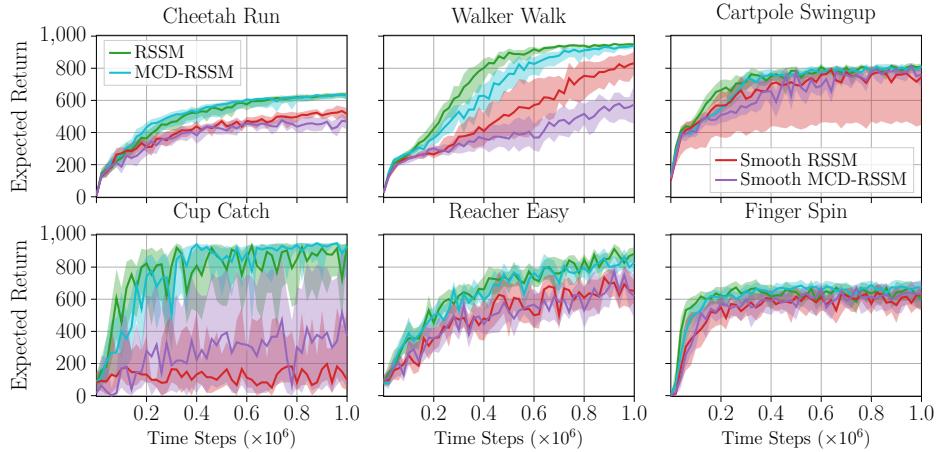
Training. We started with 5 randomly collected initial episodes and collected one more episode every 100 model update steps. Each update step is performed on 50 sub-sequences of length 50, sampled uniformly from all previously collected sequences. We used Adam (Kingma & Ba, 2015) with the same learning rates and gradient clipping as (Hafner et al., 2019) for the *PlaNet* experiments (learning rate 10^{-3}, clip by norm $1,000$) and (Hafner et al., 2020) for *Dreamer* (learning rate world model: $6 \cdot 10^{-4}$, learning rate actor and critic: $8 \cdot 10^{-5}$, all with clip by norm 100).

Environments For *PlaNet*-agents we used the same action repeats as (Hafner et al., 2019) (Cheetah Run: 4, Walker Walk: 2, Cup Catch: 4, Cartpole Swingup: 8, Reacher Easy: 4, Finger Spin: 2). For *Dreamer*-agents we used an action repeat of 2 for all environments. Images are $[64 \times 64]$ pixels and the color-depth is sub-sampled to 5-bits, following (Hafner et al., 2019). Table 1 shows splits into proprioceptive and non-proprioceptive state information for the fusion experiments.

Data Collection and Evaluation. We collected data with an exploration noise of 0.3. For the Monte-Carlo Dropout based approaches, we turned the dropout layers off during evaluation but not during data collection.

Planet-Agent The CEM-Planning method is equivalent to the one used in (Hafner et al., 2019) for all experiments.

Dreamer-Agent Actor and value networks, as well as the hyper-parameters for the generalized value estimates, are equivalent to the one used in (Hafner et al., 2020) for all approaches up to the activation function used in the value network. Here we use Tanh to avoid rare cases of exploding values for the VRKN approaches. In the cases where the original formulation with ELU converged, we observed no difference from Tanh.

Figure 12: Comparison of *RSSM* and all baselines on all tasks considered for the *PlaNet*-agents.

	RSSM	MCD-RSSM	Smooth RSSM	Smooth MCD-RSSM
Cheetah Run	627.4290 ± 7.4144	616.2516 ± 13.5786	519.9207 ± 11.7773	454.1092 ± 14.7283
Walker Walk	945.8944 ± 2.1465	912.0173 ± 19.3413	794.5836 ± 38.2716	557.6727 ± 33.9011
Cartpole Swingup	790.4359 ± 8.4232	791.2157 ± 8.4791	640.5327 ± 79.7364	761.4190 ± 10.7277
Cup Catch	783.3987 ± 54.1554	874.4680 ± 23.6101	233.3460 ± 78.0361	421.9260 ± 122.9805
Reacher Easy	862.8973 ± 8.1286	818.6773 ± 10.3870	654.9960 ± 23.2955	681.2360 ± 30.5072
Finger Spin	623.6027 ± 21.5528	635.7293 ± 32.7763	599.2760 ± 17.6737	622.0860 ± 19.4163

Table 2: Mean and standard error of final performance for the comparison of *RSSM* and all baselines on all tasks considered for the *PlaNet*-agents.

D   Comprehensive Experiment Results and Visualizations

We provide results for the individual tasks for all conducted experiments. Here we report reward curves, as well as the final performance. Following the suggestions of (Agarwal et al., 2021), for the reward curves, we report the interquartile mean and 95% bootstrapped confidence intervals (shaded areas). Unless otherwise noted, we use 10 seeds per task and approximate the expected return using 10 rollouts. We provide box plots and tables stating the mean and standard error of the final performance. We define final performance as the mean performance during the last $100,000$ train steps.

We want to emphasize that we draw our conclusion and claims from the aggregated results reported in the main part of the paper.

D.1   Comprehensive Results for the Comparison of the Different *RSSM* Versions in Section 4.1 (Figure 4)

Figure 12 shows the comparison to the Smoothing *RSSM* and the MCD versions for *PlaNet*-agents. Figure 13 and Table 2 show the corresponding box plots and table. Figure 14 shows the comparison to the Smoothing *RSSM* and the MCD versions for *Dreamer*-agents. Figure 15 and Table 3 show the corresponding box plots and table.

D.2   Comprehensive Results for *VRKN* and *RSSM* Comparison in Section 4.1 (Figure 5)

Figure 16 shows the reward curves for *PlaNet*-agents, Figure 17 and Table 4 show the corresponding box-plots and table. Figure 18 shows the reward curves for *Dreamer*-agents, Figure 19 and Table 5 show the corresponding box-plots and table.
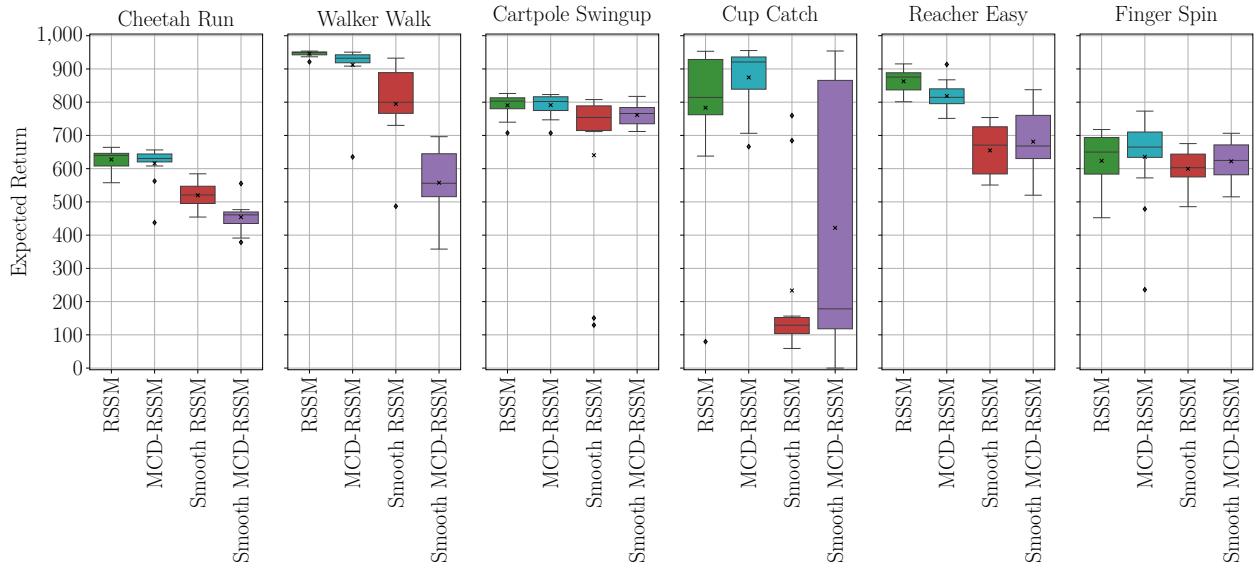
Figure 13: Box plots of final performance for the comparison of *RSSM* and all baseline on all tasks considered for the *PlaNet*-agents.
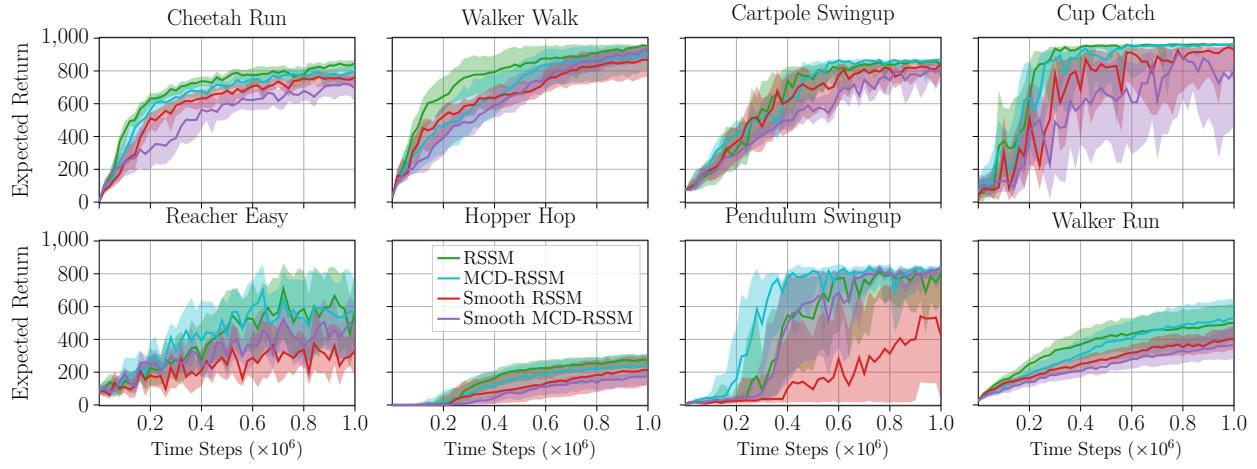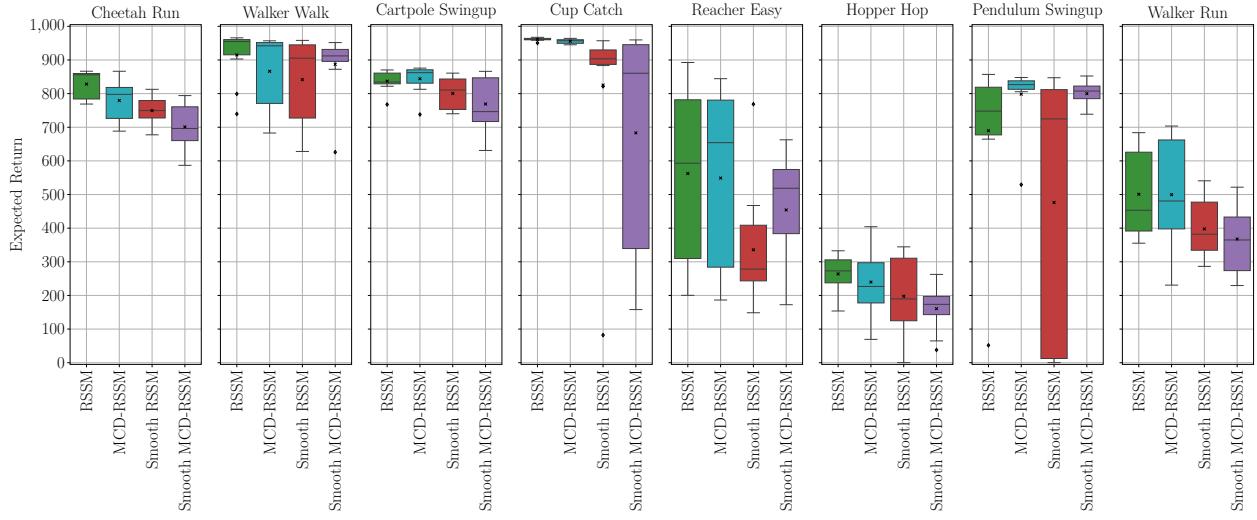

Figure 14: Comparison of *RSSM* and all baselines on all tasks considered for the *Dremaer*-agents.

D.3 Comprehensive Results for Occlusion Experiments in Section 4.2.1 (Figure 7)

Figure 20 shows the reward curves for *Dreamer*-agents on the disc occlusion task, Figure 21 and Table 6 show the corresponding box-plots and table.

Figure 22 shows the reward curves for *Dreamer*-agents on the wall occlusion task, Figure 23 and Table 7 show the corresponding box-plots and table.

D.4 Comprehensive Results for Missing Observation Experiments in Section 4.2.2 (Figure 9)

Figure 24 shows the reward curves for *Dreamer*-agents on the missing observation task without transition noise, Figure 25 and Table 8 show the corresponding box-plots and table.

Figure 26 shows the reward curves for *Dreamer*-agents on the missing observation task with transition noise, Figure 27 and Table 9 show the corresponding box-plots and table.

Figure 15: Box plots of final performance for the comparison of *RSSM* and all baseline on all tasks considered for the *Dreamer*-agents.

	RSSM	MCD-RSSM	Smooth RSSM	Smooth MCD-RSSM
Cheetah Run	828.3105 ± 12.7068	779.5831 ± 17.5038	749.6598 ± 12.6213	701.1207 ± 20.8974
Walker Walk	915.0295 ± 24.0175	866.2743 ± 33.1511	841.6051 ± 37.6502	887.1364 ± 28.4298
Cartpole Swingup	837.0084 ± 8.9790	844.2569 ± 12.9288	800.4897 ± 14.5373	769.1028 ± 23.8682
Cup Catch	961.1700 ± 1.3949	955.5520 ± 2.1011	825.4520 ± 79.2088	683.2780 ± 108.1605
Reacher Easy	562.4000 ± 80.4134	548.8700 ± 82.5122	335.7420 ± 55.2733	454.1340 ± 51.4296
Hopper Hop	263.8984 ± 17.7745	239.7520 ± 29.6752	197.5490 ± 36.8571	160.7789 ± 20.0703
Pendulum Swingup	689.7720 ± 70.8294	798.3480 ± 28.6680	476.3280 ± 121.9812	799.9800 ± 10.4065
Walker Run	500.7626 ± 39.3808	499.6024 ± 52.2246	397.7456 ± 26.9991	367.6974 ± 32.9808

Table 3: Mean and standard error of final performance for the comparison of *RSSM* and all baselines on all tasks considered for the *Dreamer*-agents.

D.5 Comprehensive Results for Sensor Fusion Experiments in Section 4.2.3 (Figure 10)

Figure 28 shows the reward curves for *Dreamer*-agents on the fusion task without transition noise, Figure 29 and Table 10 show the corresponding box-plots and table.

Figure 30 shows the reward curves for *Dreamer*-agents on the fusion task with transition noise, Figure 31 and Table 11 show the corresponding box-plots and table.

D.6 Qualitative Image Reconstructions for Noisy-Dreamer Experiments

We show sub-sequences of decoded posterior belief states for the 4 noisy tasks in Figure 32, Figure 33, Figure 34, and Figure 35. Note that the first image in those sequences is not necessary the first image the respective model saw, thus the reconstruction might be reasonable even if the system is fully occluded. Figure 36 explicitly shows the models' behavior if no information is available at the beginning of a sequence.

D.7 Further Evaluation of Stochastic Baseline from Hafner et al. (2019)

Hafner et al. (2019) give little detail about the stochastic *RSSM*-baseline (referred to as *SSM* in their work) they used. The state dimension in the official implementation defaults to 30, which is considerably smaller than the combined state size of the deterministic and stochastic parts of the *RSSM* and also smaller than the state size we used for our stochastic state. To ensure the difference in performance stems from the
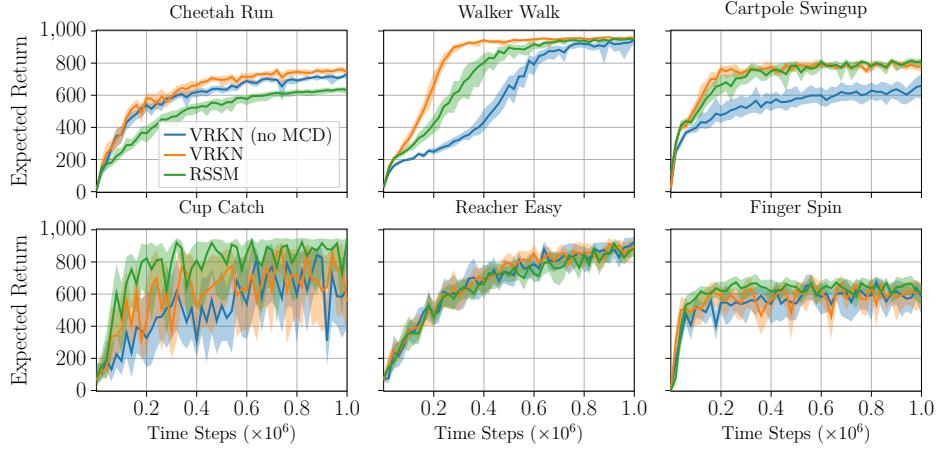
Figure 16: Comparison of *VRKN* (with and without Monte Carlo Dropout) and *RSSM* on all tasks considered for the *PlaNet*-agents.
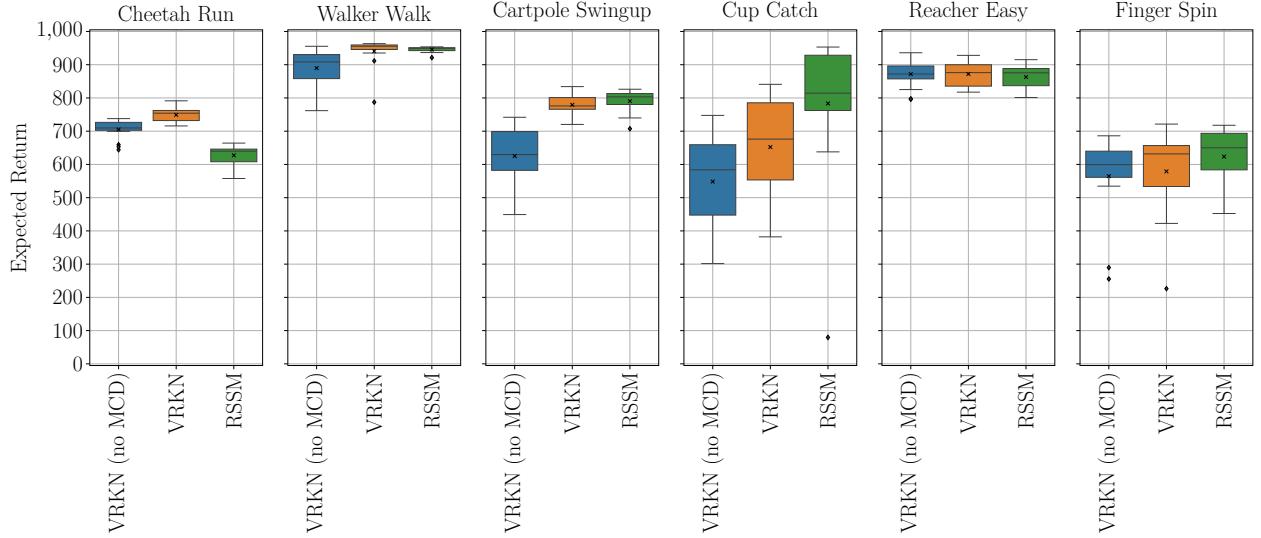

Figure 17: Box plots of final performance for the comparison of *VRKN* (with and without Monte Carlo Dropout) and *RSSM* on all tasks considered for the *PlaNet*-agents.
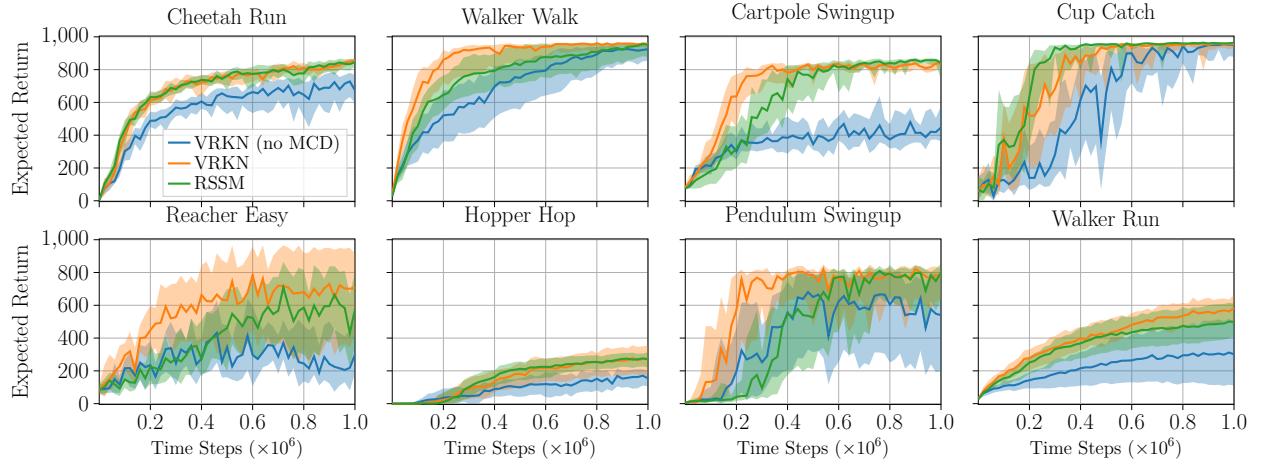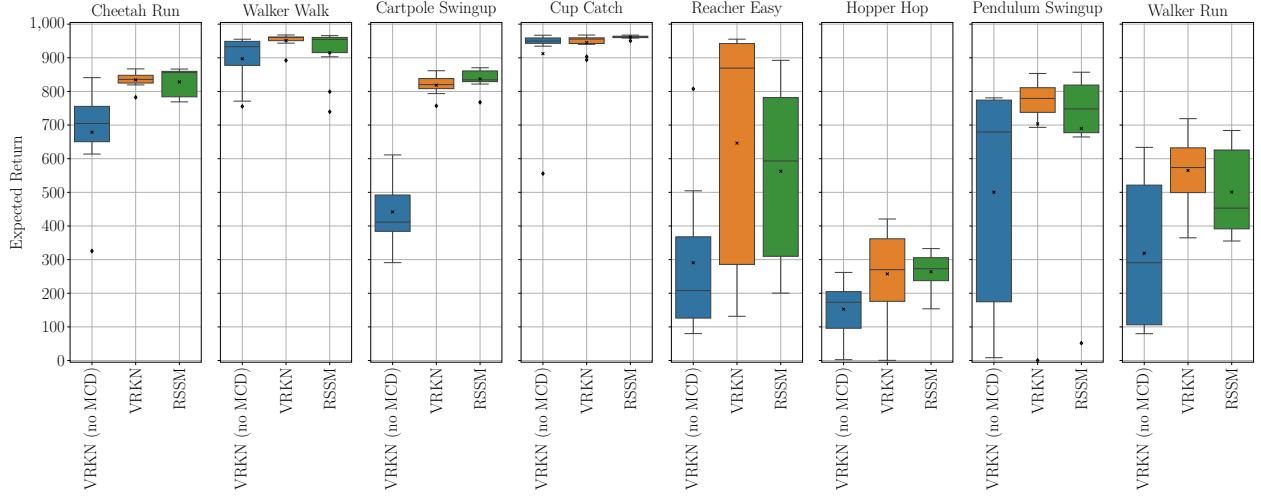
parametrization and not the reduced state size we compared the Stochastic *RSSM* baseline with state sizes of 30 and 230. We also compared a version with Bayesian treatment using Monte Carlo Dropout (MCD). The results are displayed in Figure 37 and show that neither an increased state size nor Bayesian treatment yields significant performance improvements.

	VRKN (no MCD)	VRKN	RSSM
Cheetah Run	705.1629 ± 7.3881	749.2355 ± 5.3298	627.4290 ± 7.4144
Walker Walk	889.8291 ± 14.2379	940.5245 ± 11.0899	945.8944 ± 2.1465
Cartpole Swingup	625.0746 ± 22.7305	779.3265 ± 7.7148	790.4359 ± 8.4232
Cup Catch	548.4413 ± 35.6197	652.2427 ± 37.5175	783.3987 ± 54.1554
Reacher Easy	871.8760 ± 10.4746	872.0493 ± 9.5175	862.8973 ± 8.1286
Finger Spin	564.7493 ± 31.3898	578.9867 ± 31.7433	623.6027 ± 21.5528

Table 4: Mean and standard-error of final performance for the comparison of *VRKN* (with and without Monte Carlo Dropout) and *RSSM* on all tasks considered for the *PlaNet*-agents.

Figure 18: Comparison of *VRKN* (with and without Monte Carlo Dropout) and *RSSM* on all tasks considered for the *Dreamer*-agents.

Figure 19: Box plots of final performance for the comparison of *VRKN* (with and without Monte Carlo Dropout) and *RSSM* on all tasks considered for the *Dreamer*-agents.

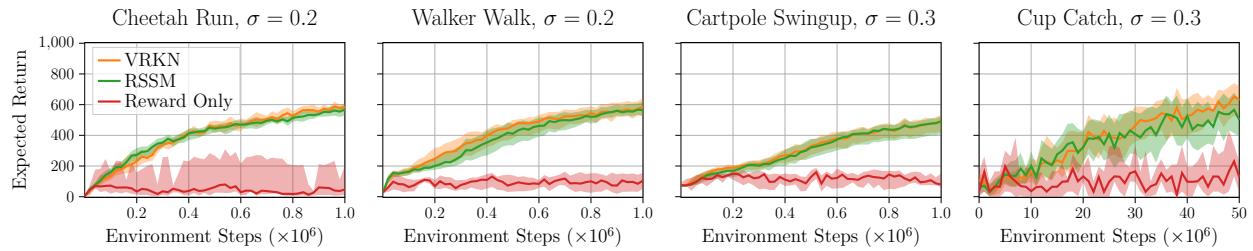|	VRKN (no MCD)	VRKN	RSSM
Cheetah Run	678.8993 ± 42.6969	834.1799 ± 7.0240	828.3105 ± 12.7068
Walker Walk	897.1648 ± 22.6760	951.5513 ± 6.6140	915.0295 ± 24.0175
Cartpole Swingup	441.9785 ± 31.5798	818.7790 ± 8.8191	837.0084 ± 8.9790
Cup Catch	912.3980 ± 37.7156	945.1860 ± 7.7854	961.1700 ± 1.3949
Reacher Easy	290.6880 ± 68.4338	646.3940 ± 106.9958	562.4000 ± 80.4134
Hopper Hop	152.6910 ± 23.3830	257.7012 ± 38.3835	263.8984 ± 17.7745
Pendulum Swingup	500.4280 ± 98.7629	703.5000 ± 75.4019	689.7720 ± 70.8294
Walker Run	318.8323 ± 68.5679	565.1005 ± 32.1744	500.7626 ± 39.3808

Table 5: Mean and standard-error of final performance corresponding for the comparison of *VRKN* (with and without Monte Carlo Dropout) and *RSSM* on all tasks considered for the *Dreamer*-agents.

Figure 20: Comparison of *VRKN* and *RSSM* on all tasks considered with disc occlusions. The σ in the title indicates the standard deviation of the Gaussian transition noise.
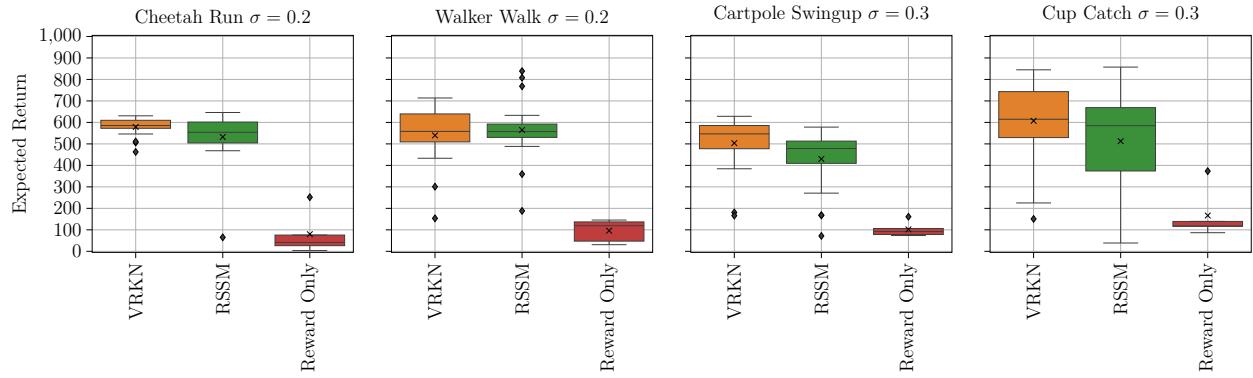
Figure 21: Box plots of final performance for the comparison of *VRKN* and *RSSM* on all tasks for the disc occlusion task.

	VRKN	RSSM	Reward Only
Cheetah Run	578.7090 ± 9.4257	532.2949 ± 26.3772	79.7795 ± 39.9028
Walker Walk	539.5958 ± 28.6619	564.8669 ± 30.8898	95.9638 ± 21.2174
Cartpole Swingup	503.7676 ± 28.6705	429.8483 ± 31.4116	102.1589 ± 14.0952
Cup Catch	607.3370 ± 40.2025	512.6090 ± 48.2354	166.6440 ± 46.7917

Table 6: Mean and standard-error of final performance for the comparison of *VRKN* and *RSSM* on all tasks for the disc occlusion task.
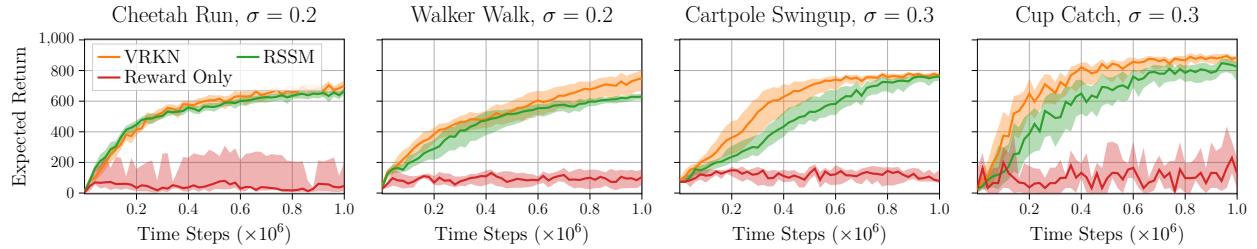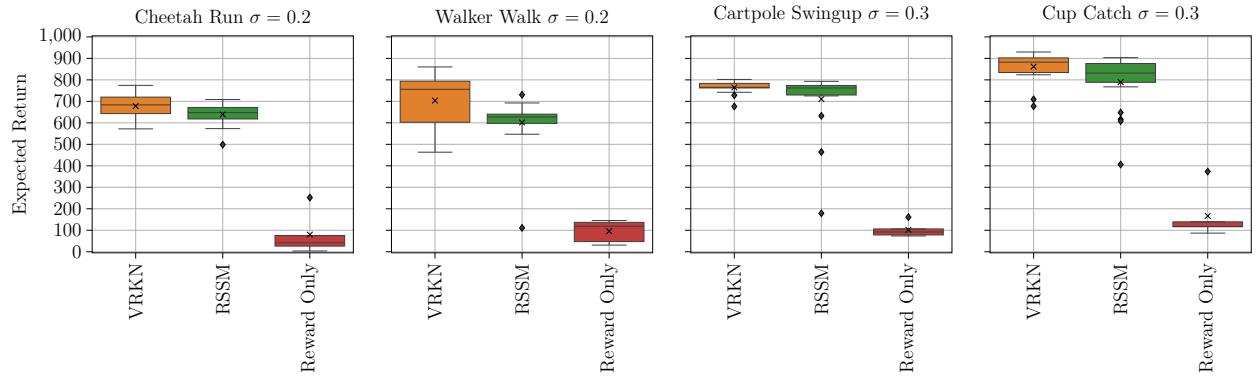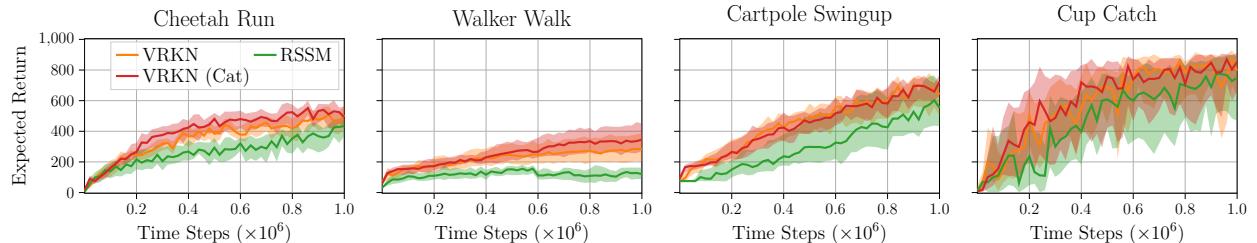
Figure 22: Comparison of *VRKN* and *RSSM* on all tasks considered with wall occlusions. The σ in the title indicates the standard deviation of the Gaussian transition noise.

Figure 23: Box plots of final performance for the comparison of *VRKN* and *RSSM* on all tasks for the wall occlusion task.

	VRKN	RSSM	Reward Only
Cheetah Run	677.8950 ± 11.7388	639.3058 ± 10.7563	79.7795 ± 39.9028
Walker Walk	703.8418 ± 27.3761	601.7267 ± 26.7561	95.9638 ± 21.2174
Cartpole Swingup	764.7615 ± 5.8841	710.6911 ± 31.6704	102.1589 ± 14.0952
Cup Catch	861.7760 ± 14.6734	789.6590 ± 27.4923	166.6440 ± 46.7917

Table 7: Mean and standard-error of final performance for the comparison of *VRKN* and *RSSM* on all tasks for the wall occlusion task.

Figure 24: Comparison of *VRKN* and *RSSM* on all tasks considered with missing observations and without transition noise.
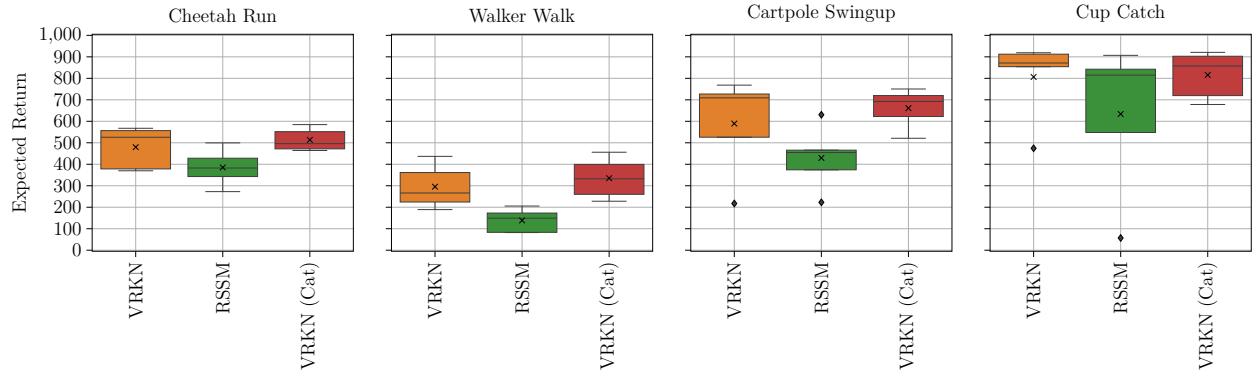
Figure 25: Box plots of final performance for the comparison of *VRKN* and *RSSM* on all tasks for the missing observation task without transition noise.

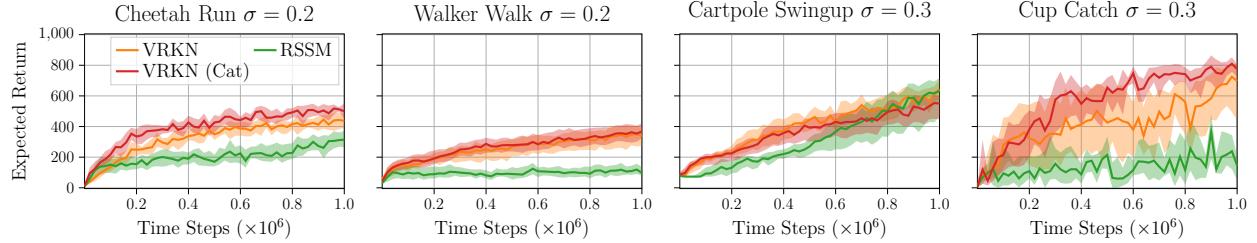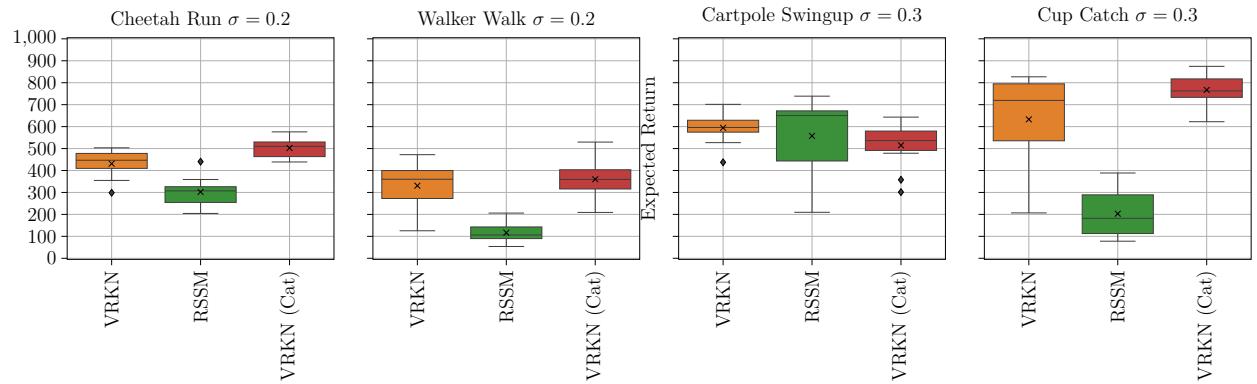|	VRKN	RSSM	VRKN (Cat)
Cheetah Run	479.6113 ± 39.0438	385.1623 ± 34.2866	513.6416 ± 20.9897
Walker Walk	295.5923 ± 40.7882	138.5695 ± 21.9475	335.1612 ± 37.8743
Cartpole Swingup	589.5229 ± 91.1411	429.4998 ± 59.3501	661.1643 ± 36.6275
Cup Catch	806.2720 ± 75.0126	633.8480 ± 140.1743	815.7960 ± 44.0564

Table 8: Mean and standard-error of final performance for the comparison of *VRKN* and *RSSM* on all tasks for the missing observation without transition noise.
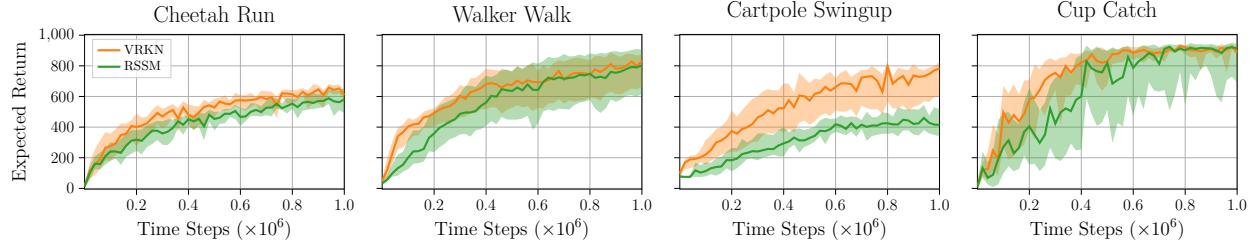

Figure 26: Comparison of *VRKN* and *RSSM* on all tasks considered with missing observations and transition noise. The σ in the title indicates the standard deviation of the Gaussian transition noise.
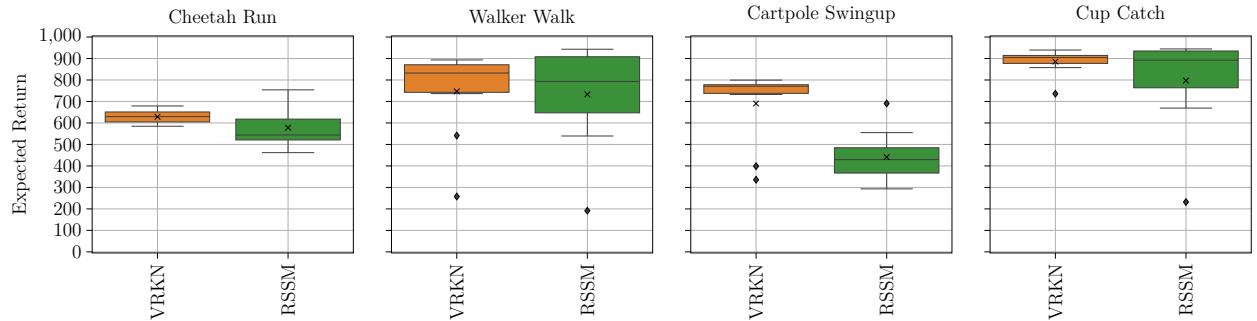

Figure 27: Box plots of final performance for the comparison of *VRKN* and *RSSM* on all tasks for the missing observation task with transition noise.

	VRKN	RSSM	VRKN (Cat)
Cheetah Run	431.1943 ± 19.2437	302.2760 ± 20.2040	502.3162 ± 13.2101
Walker Walk	330.7420 ± 30.5173	116.6937 ± 13.0846	360.0558 ± 26.1748
Cartpole Swingup	594.6512 ± 22.4822	557.7137 ± 58.3520	514.7862 ± 32.5809
Cup Catch	632.9800 ± 64.4935	203.1760 ± 32.3139	767.1400 ± 21.0592

Table 9: Mean and standard-error of final performance for the comparison of *VRKN* and *RSSM* on all tasks for the missing observation task with transition noise.

Figure 28: Comparison of *VRKN* and *RSSM* on all tasks considered for the sensor fusion task without transition noise.

Figure 29: Box plots of final performance for the comparison of *VRKN* and *RSSM* on all tasks for the sensor fusion task without transition noise.

	VRKN	RSSM
Cheetah Run	628.8849 ± 9.6539	577.7296 ± 26.4294
Walker Walk	746.9262 ± 60.4730	733.0111 ± 70.6512
Cartpole Swingup	690.6291 ± 51.6357	440.9525 ± 36.0824
Cup Catch	885.5980 ± 17.4907	797.1000 ± 66.0047

Table 10: Mean and standard-error of final performance for the comparison of *VRKN* and *RSSM* on all tasks for the sensor fusion task without transition noise.
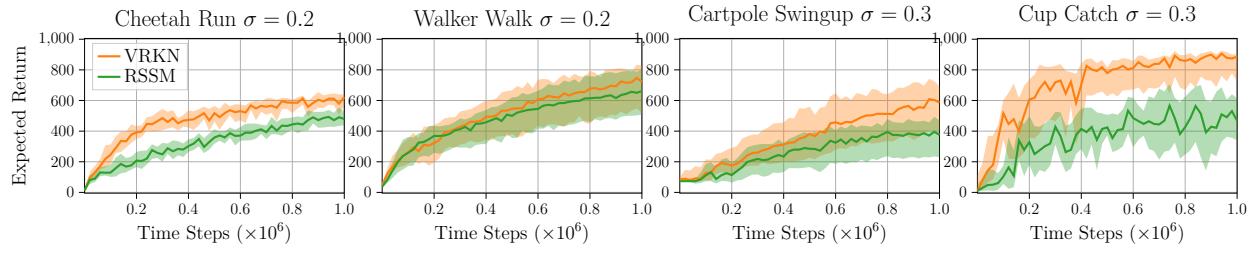
	VRKN	RSSM
Cheetah Run	594.5483 ± 13.6106	480.7173 ± 18.8966
Walker Walk	663.4760 ± 68.0791	635.1461 ± 68.1526
Cartpole Swingup	546.1525 ± 64.0839	354.1156 ± 51.2910
Cup Catch	809.5620 ± 69.0404	478.1520 ± 60.6500

Table 11: Mean and standard-error of final performance for the comparison of *VRKN* and *RSSM* on all tasks for the sensor fusion task with transition noise.

Figure 30: Comparison of *VRKN* and *RSSM* on all tasks considered for the sensor fusion task with transition noise. The σ in the title indicates the standard deviation of the Gaussian transition noise.
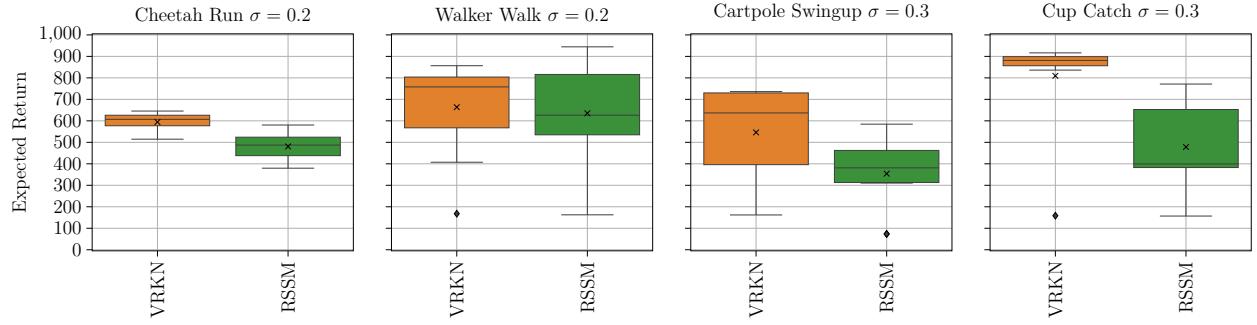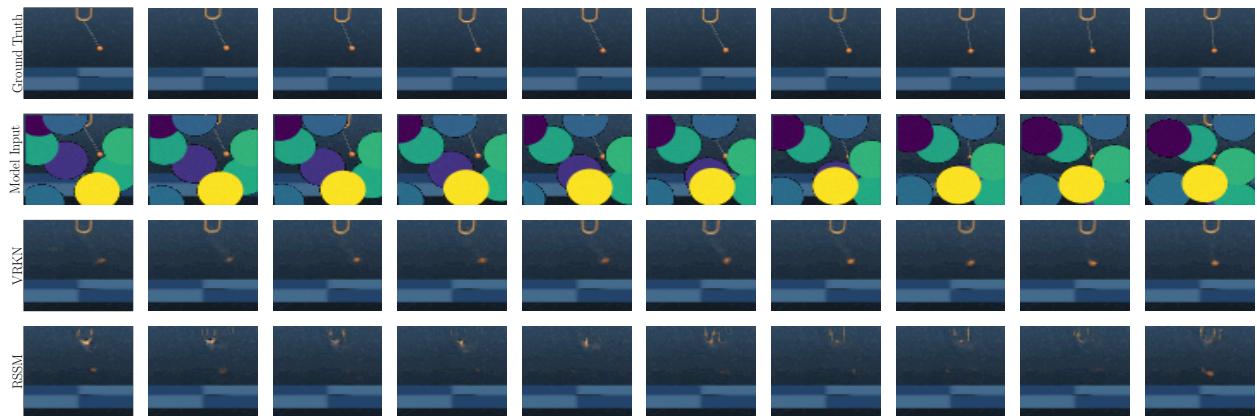

Figure 31: Box plots of final performance for the comparison of *VRKN* and *RSSM* on all tasks for the sensor fusion task with transition noise.

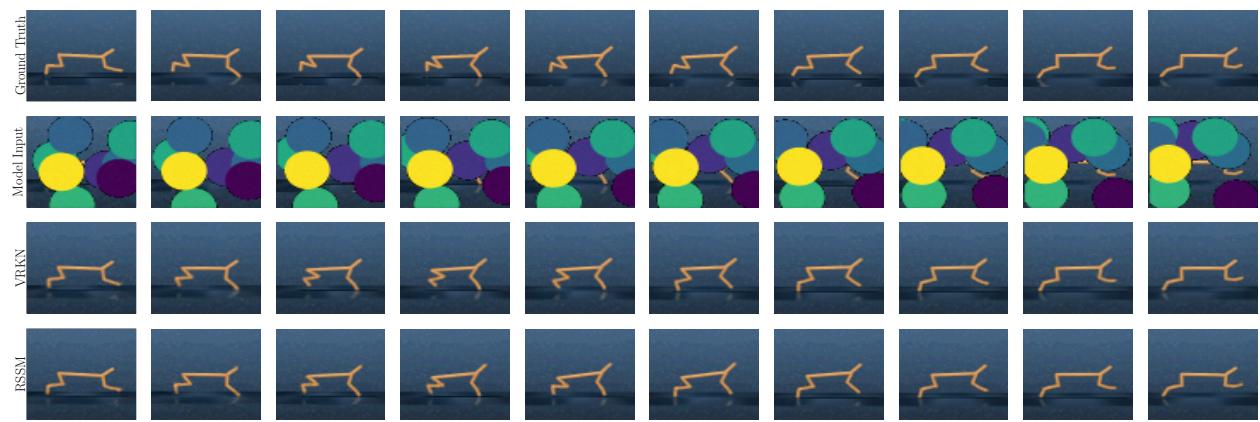Figure 32: Trajectory sample of the noisy Cup Catch task.
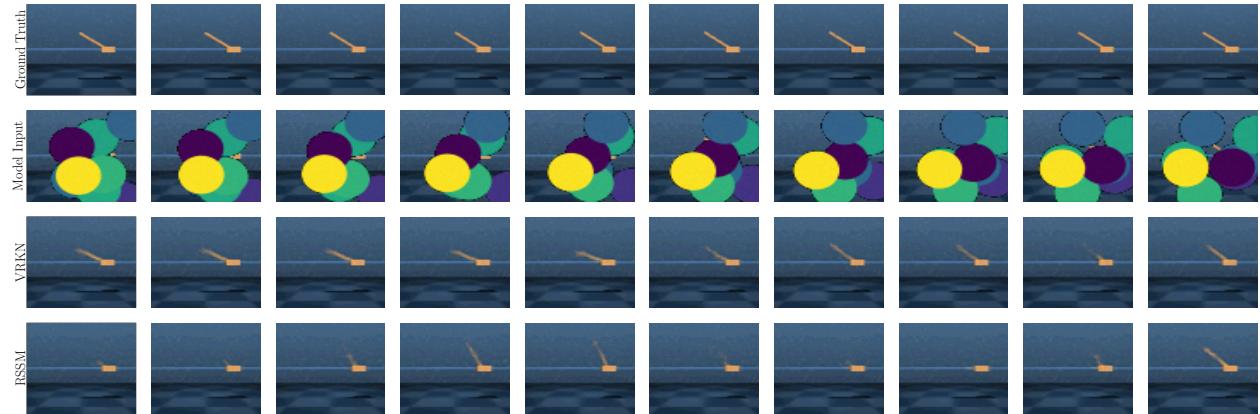
Figure 33: Trajectory sample of the noisy Cheetah Run task.

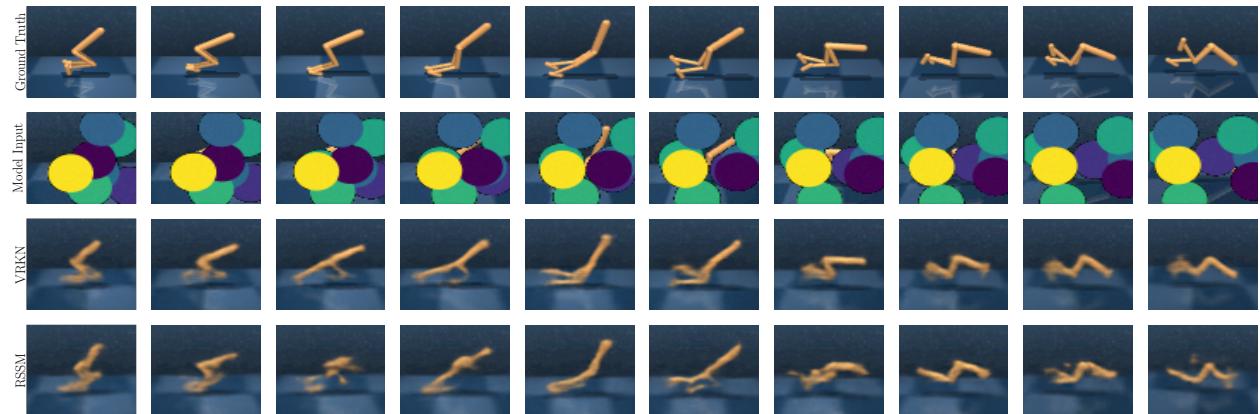Figure 34: Trajectory sample of the noisy Cartpole Swingup task.

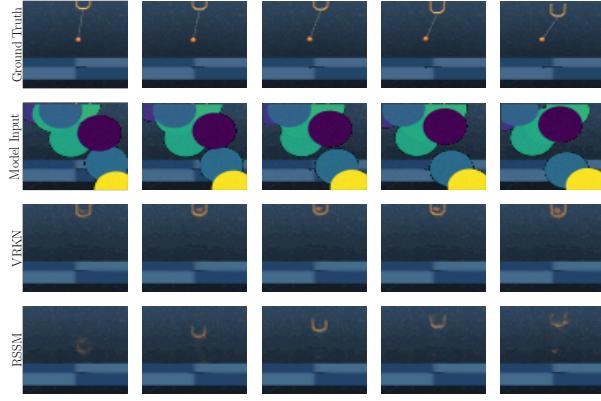Figure 35: Trajectory sample of the noisy Walker Walk task.

Figure 36: Another, sub-sequence of a cup catch trajectory. The first image shown here is the first image in the sequence. Neither the ball nor the cup is visible, i.e., the approaches have no information about their whereabouts and have to rely on their initial belief. As the model, towards the end of the agent's training, saw plenty of trajectories with caught balls, the *VRKN*'s initial belief appears reasonable. Further, the *VRKN*'s belief does only change minimally over time while the RSSM hallucinates movements without any visual information indicating them.
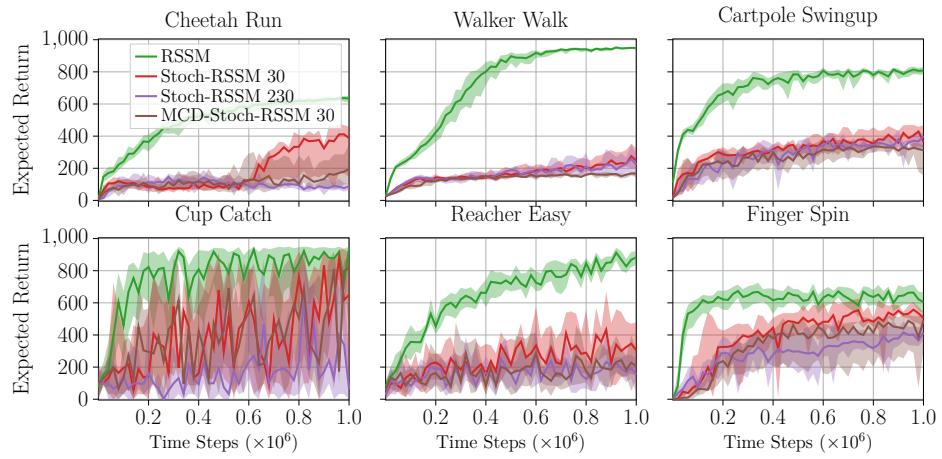

Figure 37: Evaluating of different state sizes and Bayesian treatment of the stochastic baseline introduced in (Hafner et al., 2019) using *PlaNet*-agents. Neither an increased state-size, nor Bayesian treatment increases the performance.